UAV-Assisted Satellite-Terrestrial Secure Communication Using Large-Scale Antenna Array With One-Bit ADCs/DACs

Dongxuan He, Ziyuan Sha, Han Liu, Tianqi Mao, *Member, IEEE*, and Zhaocheng Wang, *Fellow, IEEE*

***Abstract*— Unmanned aerial vehicle (UAV) equipped with large-scale antenna array constitutes a promising relaying candidate for reliable and secure satellite-terrestrial communication. Due to the limitation of energy consumption, a novel UAV architecture with one-bit analog-to-digital converters (ADCs) and one-bit digital-to-analog converters (DACs) is proposed firstly. Leveraging the additive quantization noise model, the exact closed-form expressions of both ergodic capacity and ergodic achievable secrecy rate are derived for UAV-assisted satellite-terrestrial communication systems using large-scale antenna array with one-bit ADCs/DACs. To enhance the transmission capacity and combat the eavesdropper simultaneously, maximum-ratio combining (MRC) is used by UAV to receive signals from satellite and location-based beamforming (LBB) is adopted by UAV to forward signals to destination, where the beamformer is optimized based on the derived expression of the ergodic achievable secrecy rate. Simulation results validate the accuracy of our analytical ergodic achievable secrecy rate, and demonstrate that our proposed MRC/LBB scheme has better secrecy rate than its conventional location-based counterpart.**

***Index Terms*— Satellite-aerial-terrestrial integrated network, one-bit quantization, unmanned aerial vehicle, physical layer security, beamforming.**

I. Introduction

GIVEN the ever-increasing demand for wide-area Internet of Things (IoT), flexible and seamless coverage has been regarded as an urgent need for the six-generation (6G) mobile communication network [1], [2], [3]. Inspired by its high quality, huge capacity and ubiquitous coverage, satellite can realize reliable communications with IoT devices even deployed in rural or remote areas. As a result, satellite has obtained much attention as a promising paradigm satisfying the requirements of 6G [4]. Besides that, aerial communication based on unmanned aerial vehicles (UAV) is emerging as an attractive supplement for future wireless networks due to its low cost, simple deployment and high flexibility [5], [6]. In particular, UAV is capable of connecting the satellite and terrestrial devices when the direct link is blocked, thus improving the coverage of satellite communications. Relying on the flexible deployment of UAVs and ubiquitous coverage of satellites, satellite-aerial-terrestrial integrated network offers a promising architecture providing efficient information transmission with expanded coverage and satisfied quality-of-service (QoS) [7].

A. Related Works

Due to the obstacles and shadowing between the satellite and the terrestrial destination, line-of-sight (LoS) transmissions may be blocked from time to time. To guarantee the QoS of satellite-terrestrial communications without LoS link, aerial relay has been regarded as an effective solution. Although the single-antenna UAV scheme has been investigated widely, it may not satisfy the signal-to-noise ratio (SNR) requirement over a long distance transmission [8], [9]. As an alternative solution, multi-antenna technology or large-scale antenna array are deployed at UAV to provide beamforming gain, leading to spectral efficiency improvement and performance enhancement [10], [11]. In [12], a UAV equipped with a massive antenna array was utilized to facilitate UAV-satellite communications, where stable beam was designed based on UAV navigation. In [13], when the adverse effect of knowledge imperfection is considered, including the angle of departure (AoD) caused by UAV jittering, user location uncertainty, wind speed uncertainty and polygonal no-fly zones, robust beamforming design was investigated, where the minimum SNR requirement of a multi-user downlink multi-antenna UAV communication system could be satisfied with minimum energy consumption. In [14], a three-dimensional beamforming for millimeter wave UAV communications was studied, where flexible beam coverage for any type of target area can be achieved. In [15], by jointly optimizing the beam pattern,

Manuscript received 23 May 2022; revised 12 October 2022 and 24 November 2022; accepted 24 November 2022. Date of publication 30 November 2022; date of current version 16 January 2023. This work was supported in part by the National Natural Science Foundation of China under Grant 62101306, in part by National Key R&D Program of China under Grant 2018YFB1801501, in part by Shenzhen Solving Challenging Technical Problems (JSGG20191129143216465), in part by Guangdong Optical Wireless Communication Engineering and Technology Center, and in part by Postdoctoral Science Foundation of China under Grant 2020M670332. The associate editor coordinating the review of this article and approving it for publication was A. García Armada. *(Corresponding author: Zhaocheng Wang.)*

Dongxuan He and Han Liu are with the School of Information and Electronics, Beijing Institute of Technology, Beijing 100081, China (e-mail: dongxuan_he@bit.edu.cn; liuhan4335@bit.edu.cn).

Ziyuan Sha is with Zeku Technology Corporation Ltd., Beijing 100101, China (e-mail: ne12345956@126.com).

Tianqi Mao is with the School of Electronic and Information Engineering, Beihang University, Beijing 100191, China (e-mail: maotq@buaa.edu.cn).

Zhaocheng Wang is with the Beijing National Research Center for Information Science and Technology, Department of Electronic Engineering, Tsinghua University, Beijing 100084, China, and also with the Tsinghua Shenzhen International Graduate School, Shenzhen 518055, China (e-mail: zcwang@tsinghua.edu.cn).

Color versions of one or more figures in this article are available at https://doi.org/10.1109/TCOMM.2022.3225576.

Digital Object Identifier 10.1109/TCOMM.2022.3225576

transmit power and location of UAV, the downlink sum rate of a multiple-input-multiple-output (MIMO) UAV system is maximized, showing the benefit of multi-antenna UAV in serving multiple users. For the UAV-assisted satellite-terrestrial system, large-scale antenna array is helpful to improve the reception performance and coverage capability, which can be regarded as an effective method for further improving the coverage and throughput of satellite-aerial-terrestrial integrated network.

Moreover, compared to conventional terrestrial communication, interception capability of eavesdroppers could also be enhanced due to the LoS characteristic of UAV-terrestrial links, causing non-negligible information leakage in UAV communications [16]. To address this issue, deploying multiple antennas at UAV is an effective boost for physical layer security (PLS). More specifically, multi-antenna PLS technologies, such as beamforming and artificial noise, aim to enhance the quality of the legitimate signal whilst impairing the eavesdropper signal at the same time, thus ensuring information confidentiality [17], [18]. In order to improve the secrecy rate, a multiple-antenna jammer UAV is deployed to transmit the artificial noise to degrade the quality of eavesdropping channel whilst to mitigate the interference to legitimate users [19], [20]. Besides, Q. Yuan et al. [21] investigated a location-based three dimensional beamforming of multi-antenna UAV-enabled relaying system in the presence of a multi-antenna eavesdropper, which can guarantee the QoS at the legitimate receiver and reduce the information leaked to eavesdroppers. In [22], the joint beamforming optimization of confidential signal and artificial noise signal was considered, which minimizes the total transmission power under a secrecy performance constraint.

In conclusion, multi-antenna array in improving the transmission performance and security is preferred to be deployed at UAV. However, one important factor is the energy budget of UAV, which limits its implementation significantly [23], [24]. As a result, high-resolution analog-to-digital converter (ADC) and digital-to-analog converters (DAC) are not preferred in UAVs equipped with large-scale antenna array since the power consumption, hardware cost and chip area grow exponentially with the number of quantization bits [27], [28].[1] To address this issue, one-bit quantization has been regarded as a promising technique which has the potential of reducing power consumption and implementation complexity [28], [29], [30]. For instance, Kong et al. [28] investigated a multipair massive MIMO relaying scheme with one-bit ADCs and one-bit DACs, where the achievable rate was studied, together with the optimal power allocation and power scaling law. Relying on tremendous precoding and constellation design, good performance can be obtained in multi-user multiple-input single-output (MISO) system with one-bit DACs [29]. Moreover, Z. Cheng et al. [30] explored transmit beam-pattern design in large-scale MIMO system with one-bit DACs, where directional transmission can be realized. The aforementioned works have demonstrated the feasibility of UAV using large-scale antenna array with one-bit ADCs and one-bit DACs, which motivates us to investigate the one-bit methodology for aerial relay. In consideration of information security, the secure large-scale antenna relaying in satellite-aerial-terrestrial integrated network is studied.

[1]Typically, the power consumption of a DAC/ADC with b-bits resolution can be expressed as $P_i = \text{FOM}_i f_s 2^b$ for $i \in \{\text{DAC}, \text{ADC}\}$, where FOM_i is the Walden's figure-of-merit for evaluating DAC's/ADC's power efficiency with resolution and speed, f_s is the sampling rate [25], [26]. Obviously, by reducing the quantization resolution at the DAC/ADC, the consumed power is exponentially reduced.

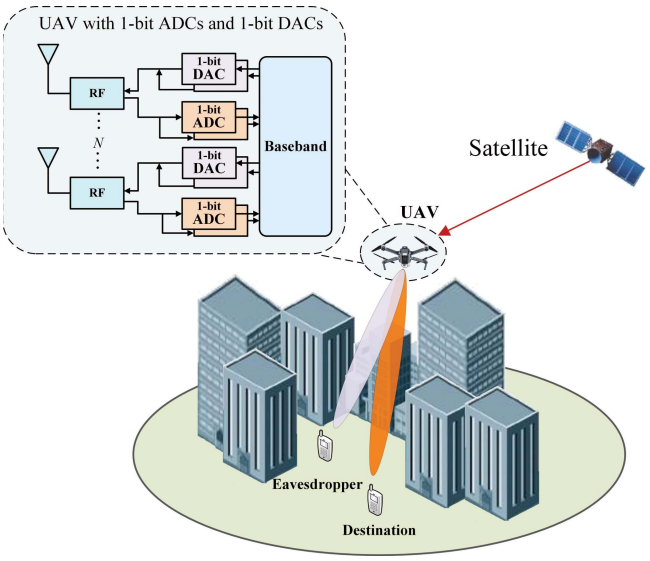

Fig. 1. System Model.

B. Main Contributions

Against the above background, we develop a novel UAV architecture with large-scale antenna array, where one-bit ADCs and one-bit DACs are equipped at UAV. Our contributions are summarized as follows

- Compared with the existing literatures regarding satellite-aerial-terrestrial integrated network, a novel UAV architecture using large-scale antenna array with one-bit ADCs/DACs is investigated firstly, where maximum-ratio combining (MRC) and location-based beamforming (LBB) are adopted at UAV to relay the signals from satellite to destination. Different from [28] that only uses Rayleigh fading to characterize the channel, shadowed-Rician fading and Rician fading are utilized to model the satellite-aerial link and aerial-terrestrial link, respectively.
- Leveraging the additive quantization noise model, the exact closed-form expression of ergodic capacity is firstly derived for the UAV-assisted satellite-terrestrial secure communication using large-scale antenna array with one-bit ADCs/DACs, which matches closely with the simulation results.
- The exact closed-form expression of the ergodic achievable secrecy rate (EASR) is derived. To improve the secrecy level of the UAV-assisted satellite-terrestrial transmission, the beamformer is optimized based on the derived ergodic achievable secrecy rate, which has better secrecy rate compared to its conventional location-based counterpart.

Notation: Matrices and vectors are denoted by uppercase and lowercase boldface letters. The expectation operator is represented by $\mathbb{E}(\cdot)$, the diagonal matrix is represented by $\text{diag}(\cdot)$, the transpose, conjugate transpose and conjugate operation are represented by $(\cdot)^T$, $(\cdot)^H$ and $(\cdot)^*$, respectively, floor and ceil function are represented by $\lfloor\cdot\rfloor$ and $\lceil\cdot\rceil$, respectively, and $\sim$ denotes the equality in a distribution. The $m \times m$ identity matrix is denoted by $\mathbf{I}_m$.

II. System Model

In this work, we consider a UAV-assisted satellite-terrestrial communication, where the geostationary orbit (GEO) satellite (S) communicates with a terrestrial destination (D) in the presence of an eavesdropper (E). Due to the shadowing effect of buildings in urban environment, the direct link between S and D (as well as E) is unavailable, where a UAV (R) hovered in the air is deployed to forward the information received from S Moreover, UAV is equipped with an antenna array with N antenna elements.[2] Multi-beam technology with single-feed-per-beam architecture is employed by S [4], [33]. Both D and E are equipped with a single antenna. Relying on visual or electronic reconnaissance, the geometrical information of the D and E, such as the distance and angle-of-departure (AoD), is assumed to be known at UAV.[3] We also assume that the channel state information (CSI) of S-R link is perfectly known at UAV, and only the statistical characteristics of the R-D link and R-E link are known at the UAV.[4]

A. S-R Link Channel Model

To describe the statistical distribution of the link from satellite to UAV, Shadowed-Rician fading model is adopted [38], [39], [40]. The channel of S-R link is modeled in consideration of the impact of satellite beam pattern, path loss, shadowing and small-scale fading, which can be expressed as [41]

$$\mathbf{h}_{SR} = \ell_{SR}\mathbf{g}_{SR}, \tag{1}$$

where ℓ_{SR} denotes the large-scale fading caused by beam pattern and path loss, given by

$$\ell_{SR} = \frac{\lambda\sqrt{G_S G_R}}{4\pi d_{SR}^{\eta_0}}, \tag{2}$$

where λ denotes the wavelength, d_{SR} denotes the distance between satellite and UAV, and η_0 denotes the path loss exponent of the satellite-UAV channel. G_S denotes the satellite beam pattern, which can be approximated as

$$G_S \approx G_S^{\max}\left(\frac{J_1(u_S)}{2u_S} + 36\frac{J_3(u_S)}{u_S^3}\right), \tag{3}$$

where $G_S^{\max}$ is the maximum gain, and $u_S = 2.07123\sin\theta_S/\sin\theta_{S,3dB}$ with θ_S representing the off-axis angle with respect to the beam boresight, and $\theta_{S,3dB}$ is the 3dB beamwidth of satellite antenna. $J_1(\cdot)$ and $J_3(\cdot)$ denote the first-kind Bessel function of order 1 and 3, respectively, and G_R is the receive antenna gain.

When the impact of shadowing and small-scale fading is considered, shadowed-Rician fading is adopted to describe the amplitude fluctuation of the signal envelope. In particular, the channel of S-R link is composed of a predominant LoS propagation path and a sparse set of multi-path components. Based on [42], $\mathbf{g}_{SR}$ can be expressed as

$$\mathbf{g}_{SR} = \mathbf{g}_{SR}^{\circ} + \mathbf{g}_{SR}^{r}, \tag{4}$$

with $\mathbf{g}_{SR}^{\circ}$ denoting the LoS component, given by

$$\mathbf{g}_{SR}^{\circ} = a_R[1, e^{j\kappa d_r \sin\theta_r}, \cdots, e^{j(N-1)\kappa d_r \sin\theta_r}]^T, \tag{5}$$

where a_R denotes a random variable following Nakagami-m distribution with average power Ω and severity parameter m. $\kappa = 2\pi/\lambda$ represents the wavenumber, θ_r represents the angle-of-arrival (AoA) of incident signal, d_r is the inter-element spacing of the array. For convenience, we consider half-wavelength spaced uniform linear array (ULA) with $d_r = \lambda/2$ is adopted. $\mathbf{g}_{SR}^{r} \in \mathbb{C}^{N\times 1}$ represents the scattering component due to multi-path effect, which is modeled as independent and identically distributed (i.i.d.) complex circular Gaussian random variable satisfying $\mathbf{g}_{SR}^{r} \sim \mathbb{CN}(\mathbf{0}, 2b\mathbf{I}_N)$ with $2b$ denoting the average power of the scattering component.

B. R-D and R-E Link Channel Model

To forward the information reliably, the connection between R and D is assumed to be guaranteed by UAV. In particular, the channel of R-D link experiences Rician fading for LoS link and Rayleigh fading for non-LoS link [43]. To characterize the LoS and multipath components of the channel $\mathbf{h}_{Rk}$ for $k \in \{D, E\}$, Rician fading combined with antenna pattern and path loss is utilized, which can be expressed as [22], [44], and [45]

$$\mathbf{h}_{Rk} = \ell_{Rk}\mathbf{g}_{Rk}, \tag{6}$$

where ℓ_{Rk} represents the large-scale loss, given by

$$\ell_{Rk}(\text{dB}) = \frac{1}{2}\left(10\lg\left(\frac{G_k + \lambda^2}{d_{Rk}^{\eta_1}}\right) - 20\lg 4\pi\right), \tag{7}$$

where η_1 denotes the path loss exponent of the UAV-terrestrial channel, d_{Rk} is the distance between UAV and k. Besides, the off-boresight antenna pattern of k is given by

$$G_k = \begin{cases} G_k^{max} 10^{-\frac{3}{10}\left(\frac{2\theta_k}{\theta_{k,3dB}}\right)^2}, & |\theta_k| \le \frac{\theta_{k,ML}}{2} \\ G_k^{SLL}, & \frac{\theta_{k,ML}}{2} \le |\theta_k| \le \frac{\pi}{2} \end{cases}, \tag{8}$$

where G_k^{max} and G_k^{SLL} denote the maximum gain and the averaged side-lobe gain of $k \in \{D, E\}$, respectively.

[2]To reduce the implementation complexity, an antenna array with a wide elevation angle is deployed along the frame arms of UAV to facilitate robust connectivity to both satellite and terrestrial destinations [31]. Besides, we assume that our considered system works at a high frequency band exemplified by Ka band, thus, large antenna array can be packed in a small area on the UAV [32].

[3]For the case that eavesdropper is an unauthorized user in the network, its location is available at UAV by some reconnaissance techniques [34], [35]. As for the case that eavesdropper's location is not available, the secure transmission scheme has also been discussed in Section V-B.

[4]The channel between satellite and UAV is assumed to be perfectly obtained by the existed channel estimation method in quantized multi-antenna systems [36], [37]. Moreover, due to the mobility of D and E, the CSI of R-D link and R-E link is hard to obtain. However, with the help of some a priori measurement campaigns, the statistical information of R-D link and R-E link, such as Rician K-factors, can be known at UAV for a determined location of D and E [34].

$\theta_{k,3dB}$ and $\theta_{k,ML}$ denote the 3dB beamwidth and main-lobe beamwidth, respectively.

Moreover, $\mathbf{g}_{Rk}$ is modeled as

$$\mathbf{g}_{Rk} = \sqrt{\frac{K_{Rk}}{K_{Rk}+1}}\mathbf{g}_{Rk}^{\circ} + \sqrt{\frac{1}{K_{Rk}+1}}\mathbf{g}_{Rk}^{r}, \tag{9}$$

where K_{Rk} denotes the Rician-K factor of the channel from UAV to k, denoting the ratio of the power between the specular component and the scattered components. In addition, $\mathbf{g}_{Rk}^{\circ} = [1, e^{j\kappa d_r \sin\theta_k}, \cdots, e^{j(N-1)\kappa d_r \sin\theta_k}]^T$ represents the LoS component with θ_k denoting the AoD from UAV to k. $\mathbf{g}_{Rk}^{r}$ represents the scattering components satisfying $\mathbf{g}_{Rk}^{r} \sim \mathbb{CN}(\mathbf{0}, \mathbf{I}_N)$.

III. UAV-Assisted Satellite-Terrestrial Transmission

In this section, we detail the secure transmission of our considered UAV-assisted satellite-terrestrial system. Considering the power limitation of UAV using large-scale antenna array, beamforming is utilized by UAV to enhance its transmission capability and information confidentiality. Furthermore, the UAV operates in half-duplex mode, where the transmission is divided into two time slots. Specifically, satellite transmits information signal x_s to UAV in this first time slot, and UAV transmits the quantized signals $\widetilde{\mathbf{x}}_R \in \mathbb{C}^{N\times 1}$ in the second time slot. The received signal at UAV and terminal k can be respectively expressed as

$$\mathbf{y}_R = \mathbf{h}_{SR}\sqrt{p_s}x_s + \mathbf{n}_R, \tag{10}$$

$$\mathrm{y}_k = \gamma \mathbf{h}_{Rk}^T \widetilde{\mathbf{x}}_R + n_k, \tag{11}$$

where p_s is the transmit power of satellite with $\mathbb{E}\left\{|x_s|^2\right\} = 1$. γ is the normalization factor in order to make the total transmit power at UAV constrained to p_r, i.e., $\mathbb{E}\left\{\|\gamma\widetilde{\mathbf{x}}_R\|^2\right\} = p_r$. $\mathbf{n}_R$ and n_k denote the i.i.d. additive white Gaussian noise (AWGN) satisfying $\mathbf{n}_R \sim \mathcal{CN}(0, \sigma_R^2\mathbf{I}_N)$ and $n_k \sim \mathcal{CN}(0, \sigma_k^2)$, where σ_R^2 and σ_k^2 are the power spectral density with respect to $\mathbf{n}_R$ and n_k, respectively.

A. UAV Reception With One-Bit ADCs

Due to the one-bit ADC architecture, the quantized received signal of UAV can be obtained according to the additive quantization noise model (AQNM), given by

$$\widetilde{\mathbf{y}}_R = \mathcal{Q}(\mathbf{y}_R) = \alpha\mathbf{y}_R + \mathbf{n}_{qa}, \tag{12}$$

where $\mathcal{Q}(\cdot)$ denotes the one-bit quantization operation, which separately processes the real and imaginary parts of the signal. Therefore, the output set of the one-bit ADCs can be expressed as $\frac{1}{\sqrt{2}}\{\pm 1 \pm 1j\}$. $\mathbf{n}_{qa}$ refers to the additive Gaussian quantization noise vector which is uncorrelated with $\mathbf{y}_R$, and α denotes a linear gain given by [46, eq.(13)]

$$\alpha = 1 - \rho = 1 - \frac{\mathbb{E}\left\{\|\widetilde{\mathbf{y}}_R - \mathbf{y}_R\|^2\right\}}{\mathbb{E}\left\{\|\widetilde{\mathbf{y}}_R\|^2\right\}}, \tag{13}$$

with ρ representing the distortion factor of the one-bit ADCs, which is around 0.3634 when one-bit quantization is adopted [47]. From (10), (12) and (13), the covariance matrix of $\mathbf{n}_{qa}$ is expressed as

$$\mathbf{R}_{\mathbf{n}_{qa}} = \alpha\rho\mathrm{diag}\left(p_s\mathbf{h}_{SR}\mathbf{h}_{SR}^H + \sigma_R^2\mathbf{I}_N\right). \tag{14}$$

B. MRC/LBB Processing

To reduce the implementation complexity, a simple amplify-and-forward (AF) protocol is adopted by UAV to process the quantized received signals, given by

$$\mathbf{x}_R = \mathbf{W}\widetilde{\mathbf{y}}_R, \tag{15}$$

where $\mathbf{W}$ denotes the processing matrix. To guarantee the low implementation complexity and superior performance at UAV, MRC is employed to handle the received signals.[5] In addition, to improve the secrecy level, LBB is utilized at the transmitter side, which can enhance the received signal at the legitimate receiver whilst degrading it at eavesdropper. The MRC/LBB processing can be expressed as $\mathbf{W} = \mathbf{w}_t\mathbf{w}_r$, where $\mathbf{w}_t$ and $\mathbf{w}_r$ are LBB and MRC vectors, respectively, formulated as [34]

$$\mathbf{w}_t = \frac{1}{\sqrt{N}}\left[1, e^{-j\kappa d_r\cos\theta_B}, \cdots, e^{-j(N-1)\kappa d_r\cos\theta_B}\right]^T, \tag{16}$$

and

$$\mathbf{w}_r = \mathbf{h}_{SR}^H, \tag{17}$$

where θ_B denotes the beamforming direction.

C. UAV Transmission With One-Bit DACs

Due to one-bit DAC architecture, the transmit signal of UAV can be expressed as

$$\widetilde{\mathbf{x}}_R = \mathcal{Q}(\mathbf{x}_R) = \alpha\mathbf{x}_R + \mathbf{n}_{qd}, \tag{18}$$

where $\mathbf{n}_{qd}$ denotes the quantization noise of one-bit DACs, which is uncorrelated with $\mathbf{x}_R$. Similar to (14), the covariance matrix of $\mathbf{n}_{qd}$ can be obtained as

$$\mathbf{R}_{\mathbf{n}_{qd}} = \alpha\rho\mathrm{diag}\left(\mathbf{R}_{\mathbf{x}_R}\right), \tag{19}$$

with $\mathbf{R}_{\mathbf{x}_R}$ denoting the covariance of $\mathbf{x}_R$, given by

$$\begin{aligned}\mathbf{R}_{\mathbf{x}_R} = \mathbb{E}\{\ \mathbf{W}\left(\alpha^2\left(p_s\mathbf{h}_{SR}\mathbf{h}_{SR}^H + \sigma_R^2\mathbf{I}_N\right)\right.\\ \left.+\alpha\rho\mathrm{diag}\left(p_s\mathbf{h}_{SR}\mathbf{h}_{SR}^H + \sigma_R^2\mathbf{I}_N\right)\right)\mathbf{W}^H\}.\end{aligned} \tag{20}$$

Since one-bit DACs is deployed in UAV with $\mathbb{E}\left\{\|\widetilde{\mathbf{x}}_R\|^2\right\} = N$, the normalization factor γ in (11) can be calculated as [28]

$$\gamma = \sqrt{\frac{p_r}{N}}. \tag{21}$$

IV. Performance Analysis

A. Secrecy Capacity Formulation

To evaluate the secrecy performance of our proposed UAV-assisted satellite-terrestrial system, ergodic secrecy capacity (ESC) is selected as the performance metric, which is defined as the maximum achievable value of the average

[5]Typically, in large antenna systems with infinite resolution ADCs, MRC will perform well with less complexity. By simply multiplying the received signals with conjugate channel coefficients, MRC is a computationally efficient scheme, thus avoiding the intractable high-dimensional matrix inversion [48]. Besides, as the number of antennas increases, MRC becomes the optimal reception strategy asymptotically, which could achieve the similar performance as zero-forcing receiver [49], [50].

secure communication rate, given by [51]

$$\mathbb{E}\{C_s\} = \mathbb{E}\left\{[C_D - C_E]^+\right\}, \tag{22}$$

where $[x]^+ = \max\{0, x\}$, C_D and C_E are the mutual information from the satellite to the destination and the eavesdropper, respectively, and $[C_D - C_E]^+$ is the secrecy capacity for one realization of the channel coefficients. Since the exact evaluation of (22) is intractable, EASR is selected as a suboptimal solution compared with ergodic secrecy capacity, which is a lower bound of (22), given by [52]

$$\overline{C}_s = [\mathbb{E}\{C_D\} - \mathbb{E}\{C_E\}]^+, \tag{23}$$

where $\mathbb{E}\{C_D\}$ and $\mathbb{E}\{C_E\}$ are the ergodic capacities of the legitimate channel and the eavesdropper channel, respectively. Based on (23), EASR can be readily obtained by calculating $\mathbb{E}\{C_D\}$ and $\mathbb{E}\{C_E\}$ corresponding to S-R-D and S-R-E links, respectively.

B. Ergodic Capacity Analysis

From (10), (11), (12), (15) and (18), the received signal at terminal k can be expressed as

$$y_k = \underbrace{\gamma\alpha^2\sqrt{p_s}\mathbf{h}_{Rk}^T\mathbf{W}\mathbf{h}_{SR}x_s}_{\text{desired signal}} + \underbrace{\widetilde{n}_k}_{\text{effective noise}}, \tag{24}$$

where $\widetilde{n}_k$ is the effective noise, given by

$$\widetilde{n}_k = \gamma\alpha^2\mathbf{h}_{Rk}^T\mathbf{W}\mathbf{n}_R + \gamma\alpha\mathbf{h}_{Rk}^T\mathbf{W}\mathbf{n}_{qa} + \gamma\mathbf{h}_{Rk}^T\mathbf{n}_{qd} + n_k. \tag{25}$$

Accordingly, the ergodic capacity of S-R-k link can be expressed as

$$\mathbb{E}\{C_k\} = \mathbb{E}\left\{\log_2\left(1 + \frac{A_k}{B_k + C_k + D_k + \sigma_k^2}\right)\right\}, \tag{26}$$

with

$$\begin{cases} A_k = \gamma^2\alpha^4 p_s|\mathbf{h}_{Rk}^T\mathbf{W}\mathbf{h}_{SR}|^2, \\ B_k = \gamma^2\alpha^4\|\mathbf{h}_{Rk}^T\mathbf{W}\|^2\sigma_R^2, \\ C_k = \gamma^2\alpha^2|\mathbf{h}_{Rk}^T\mathbf{W}\mathbf{R}_{\mathbf{n}_{qa}}\mathbf{W}^H\mathbf{h}_{Rk}^*|, \\ D_k = \gamma^2|\mathbf{h}_{Rk}^T\mathbf{R}_{\mathbf{n}_{qd}}\mathbf{h}_{Rk}^*|. \end{cases} \tag{27}$$

Since (26) is difficult to solve due to its complicated expression with the expectation of a logarithm concerning $A_k/(B_k + C_k + D_k + \sigma_k^2)$, the following lemma is introduced to simplify the analysis of ergodic capacity.

Lemma 1: When the number of antenna at the UAV is massive, the achievable ergodic capacity of S-R-k link can be approximated as

$$\begin{aligned}\mathbb{E}\{C_k\} &\approx \overline{C}_k \\ &= \log_2\left(1 + \frac{\mathbb{E}\{A_k\}}{\mathbb{E}\{B_k\} + \mathbb{E}\{C_k\} + \mathbb{E}\{D_k\} + \sigma_k^2}\right).\end{aligned} \tag{28}$$

Proof: According to [53], the following approximation always holds, given by

$$\mathbb{E}\{\log_2(1 + X/Y)\} \approx \log_2\left(1 + \mathbb{E}\{X\}/\mathbb{E}\{Y\}\right), \tag{29}$$

where $X = \sum X_i$ and $Y = \sum Y_j$ with X_i and Y_j denoting nonnegative random variables. To be noticed, X and Y are not required to be independent [53]. Accordingly, it can be obtained that $\mathbb{E}\{C_k\} \approx \log_2\left(1 + \mathbb{E}\{A_k\}/\mathbb{E}\left\{B_k + C_k + D_k + \sigma_k^2\right\}\right)$. Moreover, due to the fact that B_k, C_k, D_k, and σ_k^2 are positive variables, we have $\mathbb{E}\left\{B_k + C_k + D_k + \sigma_k^2\right\} = \mathbb{E}\{B_k\} + \mathbb{E}\{C_k\} + \mathbb{E}\{D_k\} + \sigma_k^2$. As a result, the approximation in (28) can be obtained. ■

According to **Lemma** 1, the calculation of achievable ergodic capacity can be divided into the calculations of the expectations of $\mathbb{E}\{A_k\}$, $\mathbb{E}\{B_k\}$, $\mathbb{E}\{C_k\}$ and $\mathbb{E}\{D_k\}$, thus making the calculation of ergodic capacity tractable.

C. Statistic Results

For the S-R link, the probability density function (PDF) of the squared amplitude of the channel coefficient $g_{SR,i}$ between satellite and the i-th antenna of UAV is given by [40]

$$f_{|g_{SR,i}|^2}(x) = \varphi e^{-\beta x}{}_1F_1\left(m; 1; \delta x\right), x \geq 0, \tag{30}$$

where $\varphi = (2bm/(2bm + \Omega))^m/2b$, $\beta = 1/2b$, and $\delta = \Omega/(2b)(2bm + \Omega)$. ${}_1F_1(\cdot;\cdot;\cdot)$ represents the confluent hypergeometric function of first kind [54, eq.(9.210)]. Moreover, the expectation of $|\mathbf{g}_{SR}|^2$ can be expressed as [55]

$$\mathbb{E}\{|\mathbf{g}_{SR}|^2\} = \sum_{i_1=0}^{m-1}\cdots\sum_{i_N=0}^{m-1}\Xi(N)\,\Lambda!\,(\beta - \delta), \tag{31}$$

where $\Xi(N) = \varphi^N\prod_{k=1}^N\xi(\iota_k)\prod_{j=1}^{M-1}\mathcal{B}(\sum_{l=1}^j i_l + j, i_{j+1} + 1)$, $\Lambda = \sum_{k=1}^N i_k + N$, where $\mathcal{B}(.,.)$ denotes the Beta function [54, eq.(3.351.2)], $\xi(\iota) = (-1)^\iota(1-m)_\iota\delta^\iota/(\iota!)^2$ and $(\cdot)_\iota$ denotes the Pochhhammer symbol [54, eq.(12,p.xliii)]. Here, we define $\mathbb{E}\{|\mathbf{g}_{SR}|^2\}$ as $\mathcal{G}_{SR}$ for convenience.

In addition, $\mathbb{E}\{|g_{SR,i}|^4\}$ can be calculated as [40]

$$\begin{aligned}&\mathbb{E}\{|g_{SR,i}|^4\} \\ &= \left(\frac{2bm}{2bm + \Omega}\right)^m(2b)^2\Gamma(3)\ \cdot{}_2F_1\left(3; m; 1; \frac{\Omega}{2bm + \Omega}\right),\end{aligned} \tag{32}$$

where ${}_2F_1(\cdot;\cdot;\cdot;\cdot)$ denotes the Gauss hypergeometric function [54, eq.(9.10)], and $\Gamma(\cdot)$ denotes the Gamma function [54, eq.(8.310)]. Here, we define $\mathbb{E}\{|g_{SR,i}|^4\}$ as Ψ_{SR} in the latter analysis.

Lemma 2: With beamforming direction θ_B, the expectation for the norm-square of the inner product of $\mathbf{g}_{Rk}$ and $\mathbf{w}_t$ can be expressed as

$$\mathbb{E}\{|\mathbf{g}_{Rk}^T\mathbf{w}_t|^2\} = \frac{K_{Rk}\phi^2(\theta_k, \theta_B) + N}{N(K_{Rk} + 1)}, \tag{33}$$

where $\phi(\theta_k, \theta_B) = \begin{cases} N, & \theta_k = \theta_B, \\ \frac{\sin(\frac{N\pi}{2}[\sin(\theta_k) - \sin(\theta_B)])}{\sin(\frac{\pi}{2}[\sin(\theta_k) - \sin(\theta_B)])}, & \theta_k \neq \theta_B, \end{cases}$.

Proof: Please refer to Appendix A. ■

D. Ergodic Capacity

The exact expression of the approximated ergodic capacity for the S-R-k link is given in **Theorem** 1.

Theorem 1: For the UAV-assisted satellite-terrestrial communication using large-scale antenna array with one-bit ADCs

and one-bit DACs, the closed-form expression of the approximated ergodic capacity of S-R-k link is given by

$$\overline{C}_k = \log_2\left(1 + \frac{\widetilde{A}_k}{\widetilde{B}_k + \widetilde{C}_k + \widetilde{D}_k + \sigma_k^2}\right) \tag{34}$$

with

$$\widetilde{A}_k = \mathbb{E}\{A_k\} = \gamma^2\alpha^4\ell_{SR}^4\ell_{Rk}^2 p_s \mathcal{G}_{SR}^2 \frac{K_{Rk}\phi^2(\theta_k,\theta_B)+N}{N(K_{Rk}+1)}, \tag{35}$$

$$\widetilde{B}_k = \mathbb{E}\{B_k\} = \gamma^2\alpha^4\ell_{Rk}^2\ell_{SR}^2 \mathcal{G}_{SR}\sigma_R^2 \frac{K_{Rk}\phi^2(\theta_k,\theta_B)+N}{N(K_{Rk}+1)}, \tag{36}$$

$$\widetilde{C}_k = \mathbb{E}\{C_k\} = \gamma^2\alpha^3\rho\ell_{Rk}^2\left(\ell_{SR}^4 p_s N\Psi_{SR} + \sigma_R^2\right) \times \frac{K_{Rk}\phi^2(\theta_k,\theta_B)+N}{N(K_{Rk}+1)}, \tag{37}$$

$$\widetilde{D}_k = \mathbb{E}\{D_k\} = \alpha\rho\gamma^2\ell_{Rk}^2\ell_{SR}^2 p_s\left(\alpha^2\mathcal{G}_{SR}^2 + \alpha\rho N\Psi_{SR}\right) + (\alpha^2+\alpha\rho)\rho\gamma^2\ell_{Rk}^2\sigma_R^2. \tag{38}$$

Proof: Please refer to Appendix B. ∎

Based on **Theorem** 1, a compact expression of approximated ergodic capacity can be derived as

$$\overline{C}_k = \log_2\left(\frac{\Delta_1\widetilde{\gamma}_k + \Delta_3\overline{\gamma}_k + 1}{\Delta_2\widetilde{\gamma}_k + \Delta_3\overline{\gamma}_k + 1}\right), \tag{39}$$

where $\widetilde{\gamma}_k = \frac{\overline{\gamma}_k(K\phi^2(\theta_k,\theta_B)+N)}{N(K+1)}$ with $\overline{\gamma}_k = (\gamma^2\ell_{Rk}^2)/\sigma_k^2$ denoting the average SNR at terminal k, and Δ_1, Δ_2 and Δ_3 are three parameters determined by the S-R link and quantization process, given by $\Delta_1 = \alpha^3\left[\ell_{SR}^2 p_s(\alpha\mathcal{G}_{SR}^2 + \rho N\Psi_{SR}) + \sigma_R^2\right]$, $\Delta_2 = \alpha^3\left[\rho\ell_{SR}^2 p_s N\Psi_{SR} + \sigma_R^2\right]$, and $\Delta_3 = \alpha^2\rho\big[\ell_{SR}^2 p_s \left(\alpha\mathcal{G}_{SR}^2 + \rho N\Psi_{SR}\right) + \sigma_R^2\big] + \alpha\rho^2\gamma^2\ell_{Rk}^2\sigma_R^2$.

According to (39), for a fixed terrestrial terminal k, $\overline{C}_k$ is determined by the quality of S-R link, the effect of quantization, beamforming direction θ_B and $\overline{\gamma}_k$. Specifically, for a determined S-R-k link, the channel capacity totally depends on beamforming direction θ_B. To maximize EASR, it is intuitive to select a beamforming direction that enlarges $\overline{C}_D$ and degrades $\overline{C}_E$, which will be illustrated in Section V.

Corollary 1: When MRC/MRT scheme in [52], i.e., $\mathbf{w}_t = \mathbf{h}_{RD}^H/\|\mathbf{h}_{RD}\|$*, is adopted, the ergodic capacity of S-R-k link is given by*

$$\widehat{C}_k = \log_2\left(1 + \frac{\widehat{A}_k}{\widehat{B}_k + \widehat{C}_k + \widehat{D}_k + \sigma_k^2}\right) \tag{40}$$

with

$$\widehat{A}_k = \gamma^2\alpha^4\ell_{SR}^4\ell_{Rk}^2 p_s\mathcal{G}_{SR}^2\Upsilon(k), \tag{41}$$

$$\widehat{B}_k = \gamma^2\alpha^4\ell_{Rk}^2\ell_{SR}^2\mathcal{G}_{SR}\sigma_R^2\sigma_R^2\Upsilon(k), \tag{42}$$

$$\widehat{C}_k = \gamma^2\alpha^3\rho\ell_{Rk}^2\left(\ell_{SR}^4 p_s N\Psi_{SR} + \sigma_R^2\right)\Upsilon(k), \tag{43}$$

$$\widehat{D}_k = \alpha^2\rho\gamma^2\ell_{Rk}^2\ell_{SR}^2 p_s\left(\alpha^2\mathcal{G}_{SR}^2 + \alpha\rho N\Psi_{SR}\right) + (\alpha^2+\alpha\rho)\rho\gamma^2\ell_{Rk}^2\sigma_R^2, \tag{44}$$

where

$$\Upsilon(k) = \begin{cases} \frac{2K_{RD}+1}{(K_{RD}+1)^2} + N, & k = D \\ \frac{K_{RD}K_{RE}\phi^2(\theta_D,\theta_E)+N(K_{RD}+K_{RE})+N}{N(K_{RD}+1)(K_{RE}+1)}, & k = E \end{cases}.$$

Algorithm 1 Calculation the Optimal Beamforming Direction θ_B^* and the Optimal Beamformer $\mathbf{w}_t^*$

Require: θ_D and θ_E
Ensure: θ_B^* and $\mathbf{w}_t^*$
1: Calculate Δ_1, Δ_2 and Δ_3.
2: **for** every $\theta_B \in [0,\pi]$ with step size $\Delta\theta_B$ **do**
3: Calculate $\mathbb{E}\{C_D\}$ and $\mathbb{E}\{C_E\}$ using (39).
4: Calculate $\overline{C}_s$ using (23).
5: **end for**
6: Set the beamforming direction corresponding to the maximum $\overline{C}_s$ as θ_B^*.
7: Set $\theta_B = \theta_B^*$ in (16) to obtain the optimal beamformer $\mathbf{w}_t^*$.

Intuitively, MRC/MRT is preferred to improve the channel capacity of S-R-D link. However, compared to MRC/LBB, MRC/MRT may also enhance the channel capacity of S-R-E link, thus reducing the secrecy capacity, which will be proved in Section VI. Besides, CSI of R-D link is required by MRC/MRT, which increases the implementation complexity of our proposed UAV architecture.

V. Location-Based Secure Beamforming

Based on the results in Section IV-D, the optimal location-based secure beamformer is illustrated, which maximizes EASR. Firstly, we examine the optimal beamforming vector with the knowledge of destination and eavesdropper's location. After that, the effect of Rician-K factor and the number of antennas will be discussed.

A. Optimal Location-Based Beamformer

Based on (39), the exact expression of EASR with location-based beamforming can be obtained as

$$\overline{C}_s = \left[\mathbb{E}\{C_D\} - \mathbb{E}\{C_E\}\right]^+ \approx \left[\overline{C}_D - \overline{C}_E\right]^+ = \left[\log_2\left(\frac{(\Delta_1\widetilde{\gamma}_D + \Delta_3\overline{\gamma}_D + 1)(\Delta_2\widetilde{\gamma}_E + \Delta_3\overline{\gamma}_E + 1)}{(\Delta_2\widetilde{\gamma}_D + \Delta_3\overline{\gamma}_D + 1)(\Delta_1\widetilde{\gamma}_E + \Delta_3\overline{\gamma}_E + 1)}\right)\right]^+. \tag{45}$$

To maximize EASR, the optimal location-based beamformer $\mathbf{w}_t$, which is determined by the beamforming direction, should be the one that is capable of enhancing the legitimate channel capacity while reducing the eavesdropping channel capacity. More specifically, the optimal secure beamforming direction is defined as [34]

$$\theta_B^* = \underset{0\le\theta_B\le\pi}{\operatorname{argmax}}\,\overline{C}_s. \tag{46}$$

Due to the symmetric property of the ULA, the range of θ_B is selected within $[0,\pi]$. Based on θ_B^*, the optimal beamformer $\mathbf{w}_t^*$ can be obtained by substituting θ_B^* into (16). Moreover, (46) is a one-dimensional optimization problem, which can be easily solved through finite steps of exhaustive search among all possible beamforming directions and has been presented in **Algorithm** 1.

We now evaluate the computational complexity of **Algorithm** 1 in terms of the number of floating point operations (FLOPs), where each FLOP represents one scalar

complex addition or multiplication [56]. Given Δ_1, Δ_2 and Δ_3, **Algorithm** 1 requires only $n = \lceil 2\pi/\Delta\theta_B \rceil$ calculations of (39), where the required FLOPs of each calculation is 57.[6] Moreover, we note that $\Delta\theta_B = 10^{-2}$ leads to a negligible error in maximum EASR. Assuming 4 FLOPs per cycle, 10^6 operations can be completed on a single-core 64-bit 2.5 GHz microprocessor within 1 ms [35]. As a result, **Algorithm** 1 can be performed in real-time with negligible latency impact and computational complexity.

B. User Scenarios

In this subsection, the optimal beamforming for some specific user scenarios are presented.

Proposition 1: The optimal solution to (46) *is* $\theta_B^* = \theta_D$ *in the following cases: (i) there is no line-of-sight (LoS) between UAV and eavesdropper, i.e.,* $K_E = 0$*, (ii) there are multiple spatially random-distributed eavesdroppers following Poisson point process (PPP) distributed with* Φ_e*, (iii) the location of eavesdropper is unknown.*

Proof: When $K_E = 0$, the received signal strength at E is independent of beamforming direction, and $\overline{C}_E$ is a constant. Therefore, the optimal beamforming direction turns out to be the one that maximizes $\overline{C}_D$. Moreover, it can be easily proved that $\overline{C}_D$ increases monotonically as the increase of $\widetilde{\gamma}_D$, which reaches its maximum value when $\theta_B = \theta_D$.

When there are $M \gg 0$ spatially random-distributed eavesdroppers, the problem (46) should be reformulated as [57]

$$\theta_B^* = \begin{cases} \underset{0\le\theta_B\le\pi}{\operatorname{argmax}} \underset{1\le m\le M}{\min} \left[\overline{C}_D - \overline{C}_{E_m}\right]^+, & \text{for NCE} \\ \underset{0\le\theta_B\le\pi}{\operatorname{argmax}} \left[\overline{C}_D - \overline{C}_{E,co}\right]^+, & \text{for CE,} \end{cases} \tag{47}$$

where NCE and CE represent non-colluding eavesdroppers case and colluding eavesdroppers case, respectively, $\overline{C}_{E_m} = \log_2(1 + \frac{\widetilde{A}_{E_m}}{\widetilde{B}_{E_m}+\widetilde{C}_{E_m}+\widetilde{D}_{E_m}+\sigma_{E_m}^2})$ denotes the ergodic capacity of eavesdropper m with AoD θ_{RE_m}, and $\overline{C}_{E,co} = \log_2(1 + \gamma_{E,co})$ is the eavesdropping capacity of the colluding eavesdroppers with $\gamma_{E,co} = \mathbb{E}_{\Phi_e}\left\{\sum_{m\in\Phi_e}\gamma_{E_m}\right\} = \mathbb{E}_{\Phi_e}\left\{\sum_{m\in\phi_e}\frac{\widetilde{A}_{E_m}}{\widetilde{B}_{E_m}+\widetilde{C}_{E_m}+\widetilde{D}_{E_m}+\sigma_{E_m}^2}\right\}$, where $\widetilde{A}_{E_m}$, $\widetilde{B}_{E_m}$, $\widetilde{C}_{E_m}$ and $\widetilde{D}_{E_m}$ are the parameters associated with eavesdropper m generated by (35)–(38), $\sigma_{E_m}^2$ is the noise power at eavesdropper m. For non-colluding eavesdroppers case, the maximum $\overline{C}_{E_m}$ is determined by the value of $\phi^2(\theta_{RE_m}, \theta_B)$, which is independent of θ_B since θ_{RE_m} can be arbitrary when there are multiple spatially random-distributed eavesdroppers following PPP. Similarly, for colluding eavesdroppers case, $\gamma_{E,co}$ is also a constant. When there are multiple spatially random-distributed eavesdroppers, the optimal beamforming direction is the one that maximizes $\overline{C}_D$.

When the location of eavesdropper is unknown, the ergodic capacity of S-R-E link could not be captured during the secure beamforming design. As a result, the best beamforming strategy for UAV is to enhance the legitimate channel quality. ■

[6]The calculation of (39) requires 7 additions, 10 multiplications, 4 divisions, and 3 sine operations, where the entailed FLOPs for each operation are 1, 1, 4, and 8, respectively.

Proposition 2: When there is no LoS between UAV and destination, i.e., $K_D = 0$*, the optimal beamforming direction that maximizes* $\overline{C}_s$ *is given by* $\theta_B^* = \arcsin(\sin\theta_E - 2m/N)$ *with* m *denoting an integer satisfying* $\lceil \frac{(\sin\theta_E - 1)N}{2} \rceil \le m \le \lfloor \frac{(\sin\theta_E + 1)N}{2} \rfloor$.

Proof: When $K_D = 0$, $\overline{C}_D$ is a constant since it is independent of the beamforming direction. As such, the solution of (46) is the θ_B that minimizes $\overline{C}_E$. According to (33) and (39), $\overline{C}_E$ is minimized when $\phi^2(\theta_E, \theta_B) = 0$, which can be realized by constraining $\frac{N\pi}{2}[\sin\theta_E - \sin\theta_B] = m\pi$. Besides, due to the fact that $\sin\theta_B \in [-1, 1]$, m should satisfy the requirement that $(\sin\theta_E - \frac{2m}{N}) \in [-1, 1]$. The proof is completed. ■

Proposition 3: When the number of antennas at UAV is sufficiently large, the optimal beamforming direction that maximizes $\overline{C}_s$ *is given by* $\theta_B^* = \theta_D$.

Proof: When $N \to \infty$, we have

$$\frac{K_{Rk}\phi^2(\theta_k, \theta_B) + N}{N(K_{Rk}+1)} \xrightarrow{a.s.} \begin{cases} \frac{NK_{Rk}+1}{K_{Rk}+1}, & \theta_k = \theta_B \\ \frac{1}{K_{Rk}+1}, & \theta_k \ne \theta_B, \end{cases} \tag{48}$$

where $a.s.$ denotes almost sure convergence. Obviously, $\frac{K_{Rk}\phi^2(\theta_k,\theta_B)+N}{N(K_{Rk}+1)}$ is maximized and minimized when $\theta_k = \theta_B$ and $\theta_k \ne \theta_B$, respectively. Based on (39), $\overline{C}_k$ is a monotonic increasing function of $\frac{K_{Rk}\phi^2(\theta_k,\theta_B)+N}{N(K_{Rk}+1)}$. Therefore, the optimal solution of (46) that maximizes $\overline{C}_s$ is given by $\theta_B^* = \theta_D$. ■

It is apparent that, when an antenna array with sufficient antenna elements is deployed at UAV, the beam can point towards a specified direction with negligible leakage, and the received signal at D can be further enhanced by increasing the number of antennas.

VI. Numerical Results

Numerical results are presented to validate the effectiveness of our proposed UAV architecture using large-scale antenna array with one-bit ADCs and one-bit DACs. Firstly, we verify the accuracy of our derived expression for ergodic capacity. Then, we examine the impact of beamforming direction on ergodic achievable secrecy rate and the influence of channel parameters on the optimal beamforming direction. Finally, we verify the effectiveness of our proposed **Algorithm** 1 as well as the solutions for some specific user scenarios. We assume the system works at the Ka band ($27 \sim 40$GHz), and S-R link undergoes infrequent light shadowing (ILS) with $(m, b, \Omega) = (20, 0.158, 1.29)$ [40]. The distance between satellite and UAV is $d_{SR} = 35,786$km [7], the noise power density at UAV is given by $\sigma_R^2 = \kappa_B T$ with Boltzmann constant $\kappa_B = 1.38 \times 10^{-23}$ J/K and noise temperature $T = 300$K [4]. We assume the UAV flies at a height of 800m [58], $\theta_D = \pi/3$ and $\theta_E = \pi/4$. Accordingly, we have $d_{RD} = \frac{1600}{\sqrt{3}}$m and $d_{RE} = 800\sqrt{2}$m. Furthermore, we assume the path loss exponent of S-R is $\eta_0 = 1$, and the path loss exponent of S-D link and S-E link is $\eta_1 = 2.5$ [4].

A. Accuracy Analysis

The accuracy of the expression of ergodic capacity is validated in Fig.2, where we plot $\overline{C}_D$ versus $\overline{\gamma}_D$ for different

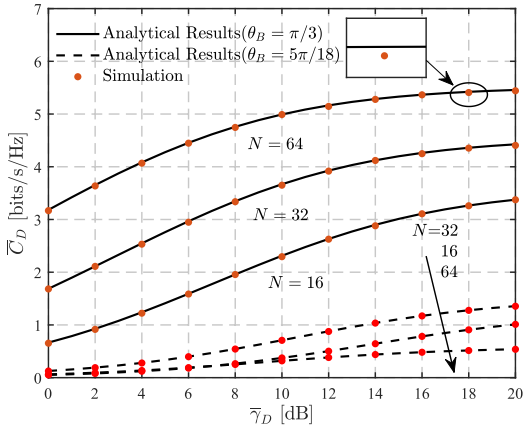

Fig. 2. Ergodic capacity $\overline{C}_D$ versus $\overline{\gamma}_D$ for different values of N with $K_{RD} = 10$dB.

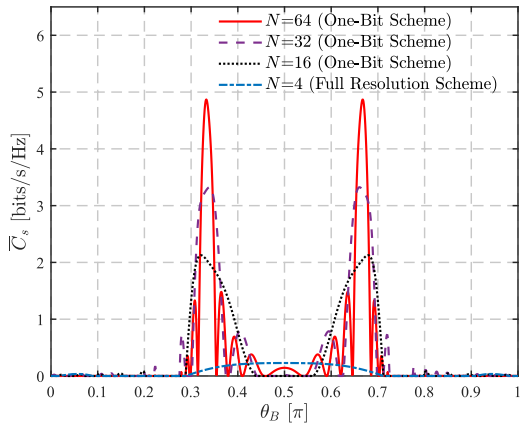

Fig. 3. Ergodic achievable secrecy rate $\overline{C}_s$ for different values of θ_B, where $K_{RD} = 10$dB, $K_{RE} = 10$dB, and $\overline{\gamma}_D = \overline{\gamma}_E = 10$dB.

values of N with $\theta_B = \pi/3$ and $\theta_B = 5\pi/18$, respectively. It is evident that the analytical curves, generated from (39), match the simulation points closely with marginal gap caused by the approximation of (28), thus validating our expression for $\overline{C}_k$ in (39). When $\overline{C}_D$ increases as the increase of $\overline{\gamma}_D$, due to the improper beamforming direction, $\overline{C}_D$ decreases obviously when $\theta_B \neq \theta_D$, which indicates that the channel capacity of S-R-E link could deteriorate seriously under mismatched beamforming direction. In addition, $\overline{C}_D$ increases as N increases when $\theta_B = \theta_D$. Therefore, when the beam generated by UAV points towards the destination, the channel capacity of S-R-D link could be improved significantly by deploying more antennas at UAV. However, when $\theta_B \neq \theta_D$, ergodic capacity achieved by $N = 64$ is smaller than $N = 32$ and $N = 16$, which indicates that more antennas may not improve the ergodic capacity when the beamforming direction does not point towards the destination.

B. Impact of Beamforming Direction

In Fig. 3, the impact of the beamforming direction θ_B on ergodic achievable secrecy rate is evaluated, where we plot $\overline{C}_s$ versus different values of θ_B with $K_{RD} = 10$dB, $K_{RE} = 10$dB and $\overline{\gamma}_D = \overline{\gamma}_E = 10$dB. We can see that there exist some

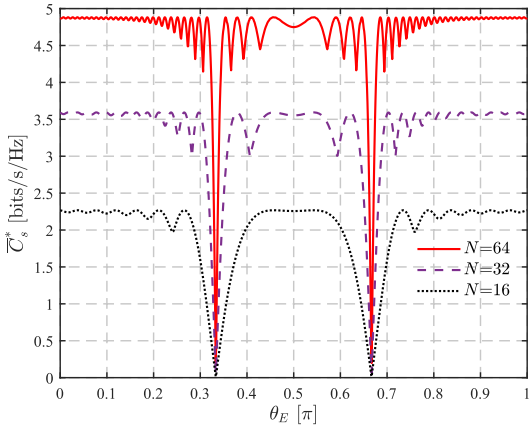

Fig. 4. Maximum ergodic achievable secrecy rate for different values of θ_E with $K_{RD} = 10$dB, $K_{RE} = 10$dB, and $\overline{\gamma}_D = \overline{\gamma}_E = 10$dB.

particular values of θ_B that maximize $\overline{C}_s$. By properly selecting the beamforming direction θ_B, the secrecy performance of our proposed UAV-assisted system could be optimized. Benefitted from the performance gain achieved by multiple antennas, with the increase of N, the achievable $\overline{C}_s$ becomes larger, indicating that it is efficient to deploy more antennas at UAV to improve the secrecy performance. However, compared to $N = 32$ and $N = 16$, $\overline{C}_s$ achieved by $N = 64$ decreases more obviously when θ_B deviates from θ_B^*. Therefore, when large-scale antenna array is deployed at UAV, the secrecy performance will deteriorate remarkably with the misaligned beamformer direction. In addition, the secrecy performance achieved by UAV with full resolution ADCs/DACs is also presented in Fig. 3, where $N = 4$. It can be observed that, compared to the full-resolution scheme with a small number of antennas, our considered one-bit scheme can improve the secrecy performance significantly by deploying more antennas, which demonstrates the effectiveness of our considered large-scale antenna array scheme using one-bit ADCs/DACs.

C. Impact of Eve's Location

In Fig. 4, the maximum ergodic achievable secrecy rate achieved by our proposed MRC/LBB scheme is plotted under different values of θ_E. Fig. 4 visually shows how the maximum ergodic achievable secrecy rate $\overline{C}_s^*$ depends on the location of eavesdropper. Moreover, regardless of eavesdropper's location, larger $\overline{C}_s^*$ can always be achieved by deploying more antennas since more energy can be concentrated on the legitimate receiver and less information will leakage to eavesdropper. As a result, it is efficient to deploy more antennas at UAV to improve the secrecy performance. Due to the fact that less signal will be leaked to eavesdropper when more antennas are deployed, the maximum $\overline{C}_s^*$ can be reached in a wider range of θ_E with larger N.

D. Impact of Channel Estimation Error

We now investigate the effect of the channel estimation error on maximum ergodic achievable secrecy rate in Fig. 5. In particular, the estimated channel $\widetilde{\mathbf{h}}_{SR}$ is modeled as [59]

$$\widetilde{\mathbf{h}}_{SR} = \sqrt{1-\epsilon}\mathbf{h}_{SR} + \sqrt{\epsilon}\Delta\mathbf{h}_{SR}, \tag{49}$$

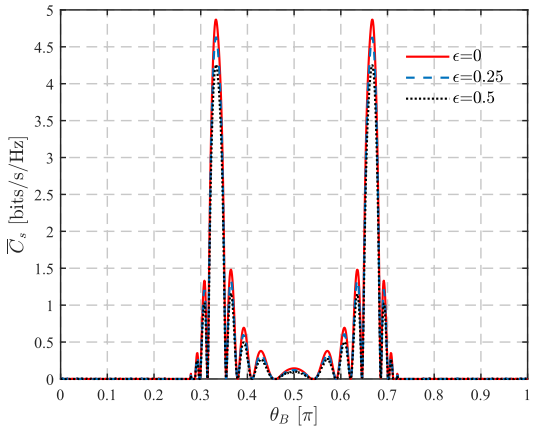

(a) $\overline{C}_s$ versus θ_B for different ϵ, where $K_{RD} = 10$dB, $K_{RE} = 10$dB, and $\overline{\gamma}_D = \overline{\gamma}_E = 10$dB.

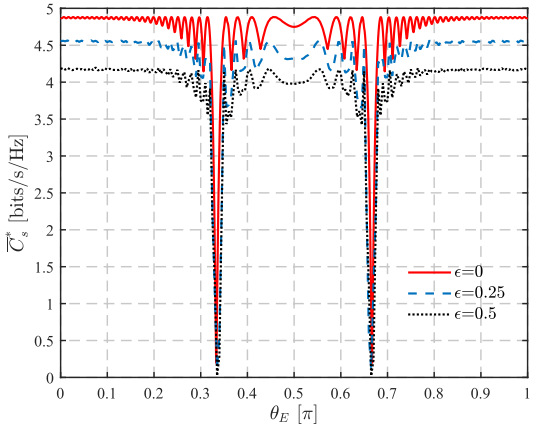

(b) $\overline{C}_s^*$ versus θ_E for different ϵ, where $K_{RD} = 10$dB, $K_{RE} = 10$dB, and $\overline{\gamma}_D = \overline{\gamma}_E = 10$dB.

Fig. 5. Secrecy performance with imperfect CSI estimation.

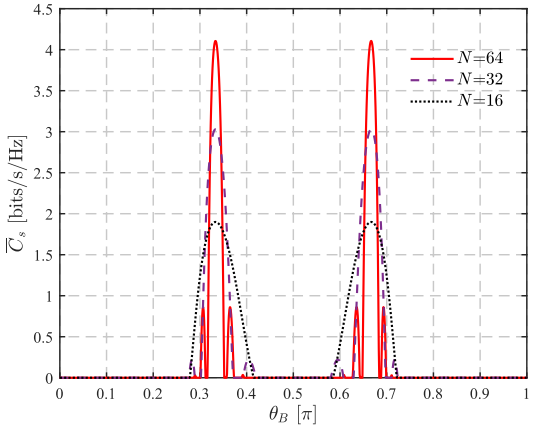

(a) $\overline{C}_s$ versus θ_B for $K_{RD} = 10$dB and $K_{RE} = 0$.

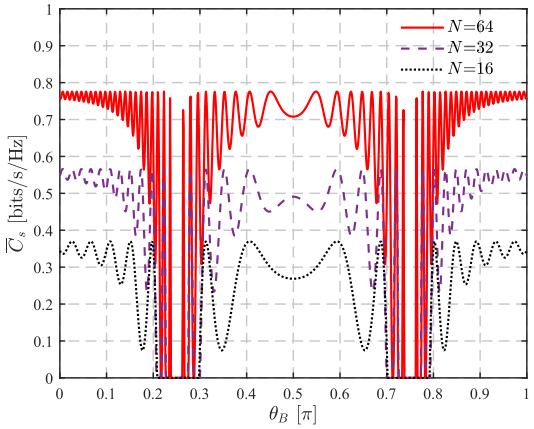

(b) $\overline{C}_s$ versus θ_B for $K_{RD} = 0$ and $K_{RE} = 10$dB.

Fig. 6. $\overline{C}_s$ versus θ_B for $K_{RD} = 0$ or $K_{RE} = 0$ with $\overline{\gamma}_D = \overline{\gamma}_E = 10$dB.

where ϵ accounts for the channel estimation factor with $\epsilon = 0$ denoting perfect CSI estimation and $\epsilon > 0$ denoting imperfect CSI estimation, and larger ϵ indicates larger CSI estimation error. $\Delta\mathbf{h}_{SR}$ is the estimation error, which is modeled as Gaussian random variables satisfying $\Delta\mathbf{h}_{SR} \sim \mathbb{CN}(\mathbf{0}, 2bl_{SR}^2\mathbf{I}_N)$. It can be observed that the secrecy performace deteriorates as the increase of CSI estimation error. However, our proposed MRC/LBB scheme can always obtain a satisfactory ergodic achievable secrecy rate even $\epsilon = 0.5$ since the capacity of legitimate channel and eavesdropping channel will deteriorate simultaneously, which demonstrates the robustness of our proposed scheme in the presence of CSI estimation error.

E. Impact of Rician-K Factor

The secrecy performance achieved by our considered UAV-assisted system for $K_{RD} = 0$ or $K_{RE} = 0$ is presented in Fig. 6. It can be seen that the proposed location-based beamforming is always efficient to improve the secrecy performance even if there is no LoS in the R-D link or R-E link. In Fig. 6(a), we plot $\overline{C}_s$ versus θ_B for $K_{RD} = 10$dB and $K_{RE} = 0$, we can see that $\overline{C}_s$ is maximized when $\theta_B = \pi/3$, which is the same as θ_D, thus verifying the correctness of **Proposition** 1. In Fig. 6(b), we plot $\overline{C}_s$ versus θ_B for $K_{RD} = 0$ and $K_{RE} = 10$dB. Obviously, compared to $K_{RD} \neq 0$, the maximum $\overline{C}_s$ degrades significantly due to the lack of LoS between UAV and destination. However, by properly selecting the beamforming direction θ_B, the secrecy performance can be enhanced, and there are multiple θ_B^* leading to the maximum $\overline{C}_s$, and the number of θ_B^* increases as N increases since $\lceil\frac{(\sin\theta_E-1)N}{2}\rceil \leq m \leq \lfloor\frac{(\sin\theta_E+1)N}{2}\rfloor$ and the number of feasible θ_B^* will increase as the increase of N. Moreover, it can be observed in Fig. 6(b) that $\theta_B^* = \arcsin(\sin\theta_E - 2m/N)$, which verifies the effectiveness of **Proposition** 2.

F. Impact of Antenna Number

In Fig. 7, we plot θ_B^* versus σ_D^2 and σ_E^2 for different N. It can be observed that the optimal beamforming direction θ_B^* is also influenced by σ_D^2 and σ_E^2. As shown in Fig. 7(a), θ_B^* tends to be $\pi/3$ when $\sigma_E^2 = 0$, while θ_B^* varies with σ_E^2 when $\sigma_D^2 = 0$. Compared with Fig. 7(a), regardless of SNR, θ_B^* is almost equal to $\pi/3$ in Fig. 7(b), which means the optimal beamforming direction is θ_B when a large-scale antenna array is deployed at UAV, thus verifying the correctness of **Proposition** 3.

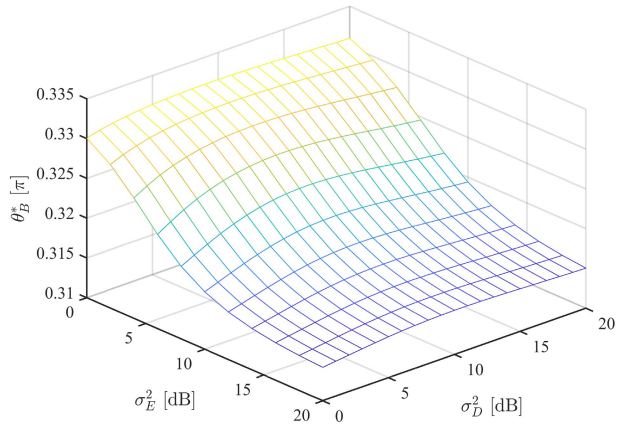

(a) θ_B^* versus σ_D^2 and σ_E^2 with N=16.

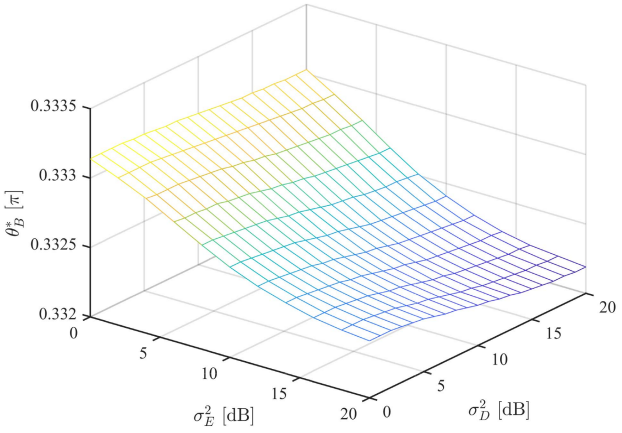

(b) θ_B^* versus σ_D^2 and σ_E^2 with N=64.

Fig. 7. θ_B^* versus σ_D^2 and σ_E^2 when $K_{RD} = 10$dB and $K_{RE} = 10$dB.

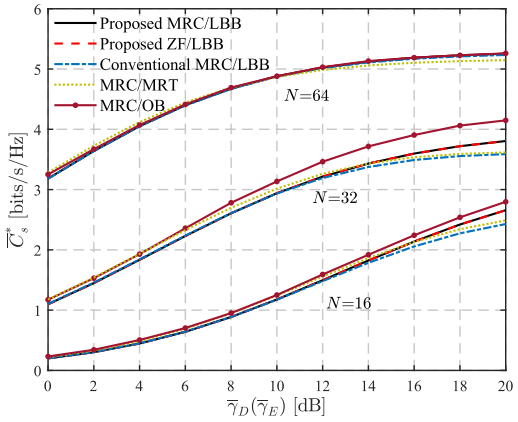

Fig. 8. Performance comparison between our proposed MRC/LBB and other counterparts.

G. Comparison of Different Schemes

In Fig. 8, we compare the secrecy performances achieved by MRC/LBB, ZF/LBB, MRC/MRT, and MRC/OB. The proposed MRC/LBB represents the location-based beamforming scheme shown in **Algorithm** 1, the proposed ZF/LBB represents the proposed location-based beamforming with zero-forcing combining shown in [49], i.e., $\mathbf{w}_r = \left(\mathbf{h}_{SR}^H \mathbf{h}_{SR}\right)^{-1} \mathbf{h}_{SR}^H$, the conventional MRC/LBB represents location-based beamforming scheme only relying on θ_D, i.e., $\theta_B = \theta_D$, and the conventional MRC/MRT represents the beamforming scheme shown in [52], i.e., $\mathbf{w}_t = \mathbf{h}_{RD}^H / \|\mathbf{h}_{RD}\|$. The MRC/OB represents the maximum-ratio combining with optimal beamforming shown in [35], i.e., $\mathbf{w}_t = \sqrt{\tau}\mathbf{w}_1 + \sqrt{1-\tau}\mathbf{w}_2$, where $\mathbf{w}_1 = \frac{\Xi_{\mathbf{g}_{Rk}^\circ}^{\perp} \mathbf{h}_{RD}^H}{\|\Xi_{\mathbf{g}_{Rk}^\circ}^{\perp} \mathbf{h}_{RD}^H\|}$ and $\mathbf{w}_2 = \frac{\Xi_{\mathbf{g}_{Rk}^\circ} \mathbf{h}_{RD}^H}{\|\Xi_{\mathbf{g}_{Rk}^\circ} \mathbf{h}_{RD}^H\|}$ with $\Xi_{\mathbf{g}_{Rk}^\circ}^{\perp} = \mathbf{I}_N - (\mathbf{g}_{Rk}^\circ)^H (\mathbf{g}_{Rk}^\circ (\mathbf{g}_{Rk}^\circ)^H)^{-1} \mathbf{g}_{Rk}^\circ$ and $\Xi_{\mathbf{g}_{Rk}^\circ} = (\mathbf{g}_{Rk}^\circ)^H (\mathbf{g}_{Rk}^\circ (\mathbf{g}_{Rk}^\circ)^H)^{-1} \mathbf{g}_{Rk}^\circ$, and τ is parameter to be optimized.

It can be seen that, with the increase of antenna array, $\overline{C}_s^*$ can be improved, which indicates that it is efficient to improve secrecy performance by deploying more antennas at UAV. Since there exists no interuser interference, the performance of proposed MRC/LBB and proposed ZF/LBB is the same in our considered UAV-assisted satellite-terrestrial communication system. Moreover, instead of only maximizing the legitimate channel capacity, our proposed MRC/LBB, which enhances the received signal at legitimate receiver whilst degrading it at eavesdropper, maximizes the ergodic achievable secrecy rate, thus achieving a better secrecy performance compared to the conventional MRC/LBB. As a result, there exists a gap between $\overline{C}_s^*$ achieved by the proposed MRC/LBB scheme and the conventional MRC/LBB when $N = 16$ and 32. However, when $N = 64$, $\overline{C}_s^*$ achieved by the proposed MRC/LBB and conventional MRC/LBB tend to be the same, which indicates that θ_B^* equals to θ_D when the number of antenna becomes large, verifying the effectiveness of **Proposition** 3. Meanwhile, due to the fact that MRC/MRT may enhance the quality of the S-R-E link, the secrecy performance achieved by MRC/MRT is not always better than our proposed MRC/LBB, while accurate CSI of R-D link is required by MRC/MRT, which increases the implementation complexity of our proposed UAV architecture. As a result, MRC/MRT is not always preferred in our considered UAV architecture with large-scale antenna array in terms of secrecy performance. Unlike MRC/MRT, which relies only on the accurate CSI of R-D link, MRC/OB also considers eavesdropper's location, thus achieving the best secrecy performance when compared to other schemes. However, due to the intractability of accurately estimating the CSI of R-D link, MRC/OB is also impractical to our proposed UAV architecture. Moreover, the secrecy performance achieved by different schemes tend to be the same when $N = 64$. As the number of antennas increases, a more directional beam towards the legitimate receiver will be generated when K_{RD} is large, which also avoids information leakage to eavesdropper. Therefore, similar secrecy performance can be achieved by different schemes when the antenna array is sufficiently large, which demonstrates the superiority of our considered LBB scheme due to the fact that accurate CSI information is not required.

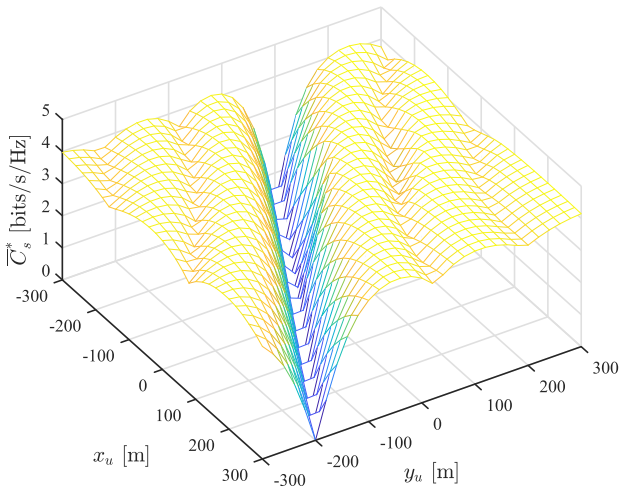

Fig. 9. Impact of UAV's location on maximum ergodic achievable secrecy rate.

H. Impact of UAV's Location

The placement of UAV has a great impact on the secrecy performance of our considered UAV system, which is shown Fig.9. In particular, we assume that the location of UAV, legitimate receiver, and eavesdropper in Cartesian coordinate system are (x_u, y_u, h_u), $(x_D, y_D, 0)$, and $(x_E, y_E, 0)$, respectively. As a result, the distance between UAV and legitimate receiver/eavesdropper can be calculated as $d_{Rk} = \sqrt{h_u^2 + (x_u - x_k)^2 + (y_u - y_k)^2}$, for $k \in \{D, E\}$. Moreover, we assume that the UAV is hovering at a fixed height $h_u = 800$m, the locations of legitimate receiver and eavesdropper are $(200\text{m}, 0, 0)$ and $(-200\text{m}, -200\text{m}, 0)$, respectively, and $\overline{\gamma}_k = 20$dB when $d_{Rk} = 800$m. It is evident that the maximum ergodic achievable secrecy rate changes as the variation of UAV's locations, which is due to the fact that the received signal strength at both the legitimate receiver and the eavesdropper is highly determined by the UAV location. By properly designing UAV's location, the received signal strength at legitimate receiver and eavesdropper can be enhanced and reduced, which might improve the transmission security.

I. Impact of Receiver's Mobility

Finally, we examine the effect of legitimate receiver's mobility on secrecy performance. In particular, the Ornstein-Uhlenbeck (OU) process is adopted to characterize the random movement of legitimate receiver, given by [60]

$$\mathrm{d}S(t) = \frac{1}{\varsigma}(S_d - S(t))\mathrm{d}t + \sqrt{D}\mathrm{d}W(t), \tag{50}$$

where S_d is the desired location of legitimate receiver, $W(t)$ represents the Wiener process. The parameters ς and D are positive constants called the relaxation time and the diffusion coefficient, respectively, where $\sqrt{D}$ controls the location fluctuation and $1/\varsigma$ determines the rate of reversion of the receiver to its desired location S_d.

In Fig. 10, we plot $\overline{C}_s$ versus ς for different D when legitimate receiver and eavesdropper are moving. We assume that the location of UAV is $(0, 0, 800\text{m})$, the initial and desired locations of legitimate receiver are $(100\text{m}, 0, 0)$ and $(200\text{m}, -100\text{m}, 0)$, respectively, the initial and desired locations of legitimate receiver are and $(-200\text{m}, -200\text{m}, 0)$ and $(100\text{m}, 0, 0)$, respectively. Moreover, we assume that UAV detects the location information of receivers every second and then determines its beamformer. It can be observed that, $\overline{C}_s$ decreases significantly as the increase of $1/\varsigma$ and D, which indicates that the secrecy performance will deteriorate due to receiver's mobility. Therefore, to ensure the effectiveness of our proposed scheme, UAV should update the location information of receivers timely.

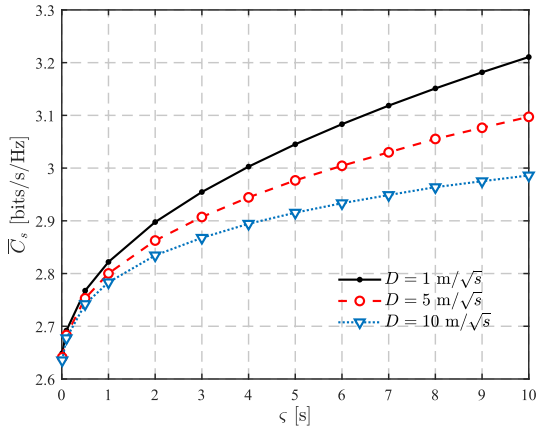

(a) $\overline{C}_s$ versus ς when legitimate receiver is moving.

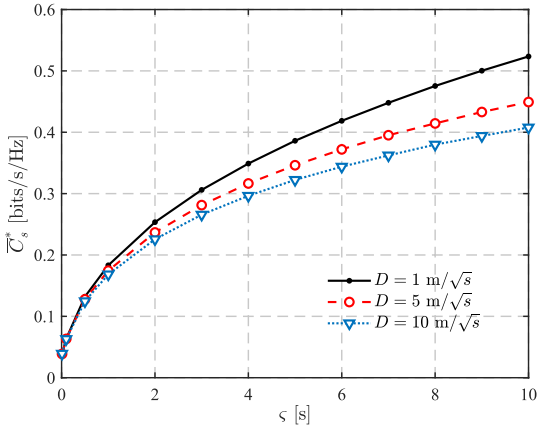

(b) $\overline{C}_s$ versus ς when eavesdropper is moving.

Fig. 10. Impact of receiver's mobility on ergodic achievable secrecy rate.

VII. Conclusion

In this paper, to satisfy the energy limitation of UAV equipped with large-scale antenna array, a novel UAV architecture with one-bit ADCs and one-bit DACs was proposed to facilitate secure satellite-terrestrial communication. Based on additive quantization noise model, the exact expressions for both ergodic capacity and ergodic achievable secrecy rate were derived to facilitate the design of secure beamformer. Aiming at enhancing the transmission capacity and secrecy rate at the same time, maximum-ratio combining and location-based beamforming were implemented at UAV to handle the received signal from satellite, where the beamforming direction was

optimized in accordance with the derived ergodic achievable secrecy rate. Simulation results demonstrated that, by properly selecting the beamformer, our proposed MRC/LBB scheme is capable of achieving a better secrecy performance compared to its conventional location-based counterpart.

APPENDIX A
PROOF OF LEMMA 2

For analytical simplicity, the following definitions are provided

$$e^{j(n-1)\kappa d_r \sin\theta_\nu} = \varrho^c_{\nu n} + j\varrho^s_{\nu n}, \quad \nu \in \{D, E, B\},$$
$$g_{Rk,n} = s_{kn} + jt_{kn}, \quad k \in \{D, E\}, \tag{51}$$

where $\varrho^c_{kn} = \cos\left((n-1)\kappa d_r \sin\theta_k\right)$ and $\varrho^s_{kn} = \sin\left((n-1)\kappa d_r \sin\theta_k\right)$ are the real and imaginary parts of $e^{j(n-1)\kappa d_r \sin\theta_k}$, $g_{Rk,n}$ is the n-th entry of $\mathbf{g}_{Rk}$, and s_{kn} and t_{kn} represent the independent real and imaginary parts of $g_{Rk,n}$.

To obtain the expectation for the norm-square of the inner product of $\mathbf{g}_{Rk}$ and $\mathbf{w}_t$, both the real and imaginary parts of $\mathbf{g}^T_{Rk}\mathbf{w}_t$ should be extracted, where the expectation can be formulated as [53]

$$\mathbb{E}\left\{|\mathbf{g}^T_{Rk}\mathbf{w}_t|^2\right\} = \mathbb{E}\left\{\left(\mathbf{g}^T_{Rk}\mathbf{w}_t\right)^2_{\text{real}} + \left(\mathbf{g}^T_{Rk}\mathbf{w}_t\right)^2_{\text{imag}}\right\}. \tag{52}$$

If $\theta_B = \theta_k$, we have

$$\begin{aligned}&\mathbf{g}^T_{Rk}\mathbf{w}_t \\ &= \left(\sqrt{\frac{K_{Rk}}{K_{Rk}+1}}\mathbf{g}^{oT}_{Rk} + \sqrt{\frac{1}{K_{Rk}+1}}\mathbf{g}^{rT}_{Rk}\right)\mathbf{g}^{\circ *}_{Rk} \\ &= \frac{1}{\sqrt{K_{Rk}+1}}\sum_{n=1}^{N}\left(\sqrt{K_{Rk}N} + (s_{kn}+jt_{kn})(\varrho^c_{Bn} - j\varrho^s_{Bn})\right).\end{aligned} \tag{53}$$

Accordingly, the real and imaginary parts can be respectively expressed as

$$\left(\mathbf{g}^T_{Rk}\mathbf{w}_t\right)_{\text{real}} = \sqrt{\frac{1}{K_{Rk}+1}}\left(\sum_{n=1}^{N}(s_{kn}\varrho^c_{Bn} + t_{kn}\varrho^s_{Bn}) + \sqrt{K_{Rk}N}\right), \tag{54}$$

$$\left(\mathbf{g}^T_{Rk}\mathbf{w}_t\right)_{\text{imag}} = \sqrt{\frac{1}{K_{Rk}+1}}\left(\sum_{n=1}^{N}(t_{kn}\varrho^c_{Bn} - s_{kn}\varrho^s_{Bn})\right). \tag{55}$$

Substituting (54) and (55) into (52) and removing the terms with zero expectation, we get the result of the case $\theta_B = \theta_k$ as

$$\mathbb{E}\{|\mathbf{g}^T_{Rk}\mathbf{w}_t|^2\} = \frac{K_{Rk}N+1}{K_{Rk}+1}. \tag{56}$$

In addition, if $\theta_B \neq \theta_k$, we have

$$\begin{aligned}&\mathbf{g}^T_{Rk}\mathbf{w}_t \\ &= \left(\sqrt{\frac{K_{Rk}}{K_{Rk}+1}}\mathbf{g}^{oT}_{Rk} + \sqrt{\frac{1}{K_{Rk}+1}}\mathbf{g}^{rT}_{Rk}\right)\mathbf{w}_t \\ &= \sqrt{\frac{1}{N(K_{Rk}+1)}}\sum_{n=1}^{N}\Big(\sqrt{K_{Rk}}\,(\varrho^c_{kn} + j\varrho^s_{kn})(\varrho^c_{Bn} - j\varrho^s_{Bn}) \\ &\quad + (s_{kn} + jt_{kn})(\varrho^c_{Bn} - j\varrho^s_{Bn})\Big).\end{aligned} \tag{57}$$

Applying the fact that $\sum_{n=1}^{N} e^{j(n-1)\pi[\sin(\theta_j)-\sin(\theta_i)]} = \phi(\theta_n,\theta_i)e^{j(N-1)\pi[\sin(\theta_j)-\sin(\theta_i)]}$ [61, eq.(14)], the real and imaginary parts can be respectively expressed as

$$\begin{aligned}&\left(\mathbf{g}^T_{Rk}\mathbf{w}_t\right)_{\text{real}} \\ &= \sqrt{\frac{1}{N(K_{Rk}+1)}}\Bigg(\sum_{n=1}^{N}(s_{kn}\varrho^c_{Bn} + t_{kn}\varrho^s_{Bn}) + \\ &\quad \sqrt{K_{Rk}}\phi(\theta_k,\theta_B)\cos\left(\frac{N-1}{2}\pi[\sin(\theta_k)-\sin(\theta_B)]\right)\Bigg),\end{aligned} \tag{58}$$

$$\begin{aligned}&\left(\mathbf{g}^T_{Rk}\mathbf{w}_t\right)_{\text{imag}} \\ &= \sqrt{\frac{1}{N(K_{Rk}+1)}}\Bigg(\sum_{n=1}^{N}(t_{kn}\varrho^c_{Bn} - s_{kn}\varrho^s_{Bn}) + \\ &\quad \sqrt{K_{Rk}}\phi(\theta_k,\theta_B)\sin\left(\frac{N-1}{2}\pi[\sin(\theta_k)-\sin(\theta_B)]\right)\Bigg).\end{aligned} \tag{59}$$

Substituting (58) and (59) into (52) and removing the terms with zero expectation, we get the final result as

$$\mathbb{E}\left\{|\mathbf{g}^T_{Rk}\mathbf{w}_t|^2\right\} = \frac{K_{Rk}\phi^2(\theta_k,\theta_B)+N}{N(K_{Rk}+1)}. \tag{60}$$

APPENDIX B
PROOF OF THEOREM 1

The end-to-end capacity given in (34) consists of four expectation terms: 1) desired signal A_k; 2) noise at the relay B_k; 3) quantization noise of ADCs C_k; 4) quantization noise of DACs D_k. We compute them one by one as follows.

1) Calculation of $\widetilde{A}_k$: Since

$$\begin{aligned}\mathbb{E}\{A_k\} &= \gamma^2\alpha^4 p_s \mathbb{E}\left\{|\mathbf{h}^T_{Rk}\mathbf{W}\mathbf{h}_{SR}|^2\right\} \\ &= \gamma^2\alpha^4\ell^2_{SR}\ell^2_{Rk}p_s\mathbb{E}\left\{|\mathbf{g}^T_{Rk}\mathbf{w}_t|^2\right\}\mathbb{E}\left\{|\mathbf{w}_r\mathbf{g}_{SR}|^2\right\},\end{aligned} \tag{61}$$

the expectation of A_k can be obtained, given by

$$\mathbb{E}\{A_k\} = \gamma^2\alpha^4\ell^4_{SR}\ell^2_{Rk}p_s\mathcal{G}^2_{SR}\frac{K_{Rk}\phi^2(\theta_k,\theta_B)+N}{N(K_{Rk}+1)}. \tag{62}$$

2) Calculation of $\widetilde{B}_k$:

$$\begin{aligned}\mathbb{E}\{B_k\} &= \gamma^2\alpha^4\ell^2_{Rk}\sigma^2_R\mathbb{E}\left\{|\mathbf{g}^T_{Rk}\mathbf{w}_t|^2\|\mathbf{h}^H_{SR}\|^2\right\} \\ &= \gamma^2\alpha^4\ell^2_{Rk}\ell^2_{SR}\mathcal{G}_{SR}\sigma^2_R\frac{K_{Rk}\phi^2(\theta_k,\theta_B)+N}{N(K_{Rk}+1)}.\end{aligned} \tag{63}$$

3) Calculation of $\widetilde{C}_k$:

$$\begin{aligned}\mathbb{E}\left\{C_k\right\} &= \gamma^2\alpha^2\mathbb{E}\left\{\left|\mathbf{h}_{Rk}^T\mathbf{W}\mathbf{R}_{\mathbf{n}_{qa}}\mathbf{W}^H\mathbf{h}_{Rk}^*\right|\right\} \\ &= \gamma^2\alpha^2\ell_{Rk}^2\mathbb{E}\left\{\left|\mathbf{g}_{Rk}^T\mathbf{w}_t^T\mathbb{E}\left\{\mathbf{w}_r\mathbf{R}_{\mathbf{n}_{qa}}\mathbf{w}_r^H\right\}\mathbf{w}_t^*\mathbf{g}_{Rk}^*\right|\right\},\end{aligned} \tag{64}$$

where

$$\begin{aligned}\mathbb{E}\{\mathbf{w}_r\mathbf{R}_{\mathbf{n}_{qa}}\mathbf{w}_r^H\} &= \alpha\rho\left(\mathbb{E}\left\{\mathbf{w}_r\text{diag}\left(p_s\mathbf{h}_{SR}\mathbf{h}_{SR}^H\right)\mathbf{w}_r^H\right\}+\sigma_R^2\right) \\ &= \alpha\rho\left(\ell_{SR}^2p_s\mathbb{E}\left\{\sum_{n=1}^{N}|g_{SR,n}|^4\right\}+\sigma_R^2\right) \\ &= \alpha\rho(\ell_{SR}^2p_sN\Psi_{SR}+\sigma_R^2).\end{aligned} \tag{65}$$

Substituting (65) into (64), $\mathbb{E}\left\{C_k\right\}$ can be obtained, given by

$$\begin{aligned}&\mathbb{E}\left\{C_k\right\} \\ &= \gamma^2\alpha^3\rho\ell_{Rk}^2\left(\ell_{SR}^4p_sN\Psi_{SR}+\sigma_R^2\right)\frac{K_{Rk}\phi^2(\theta_k,\theta_B)+N}{N(K_{Rk}+1)}.\end{aligned} \tag{66}$$

4) Calculation of $\widetilde{D}_k$:

$$\begin{aligned}&\mathbb{E}\left\{D_k\right\} \\ &= \gamma^2\mathbb{E}\left\{\left|\mathbf{h}_{Rk}^T\mathbf{R}_{\mathbf{n}_{qd}}\mathbf{h}_{Rk}^*\right|\right\} \\ &= \alpha\rho\gamma^2\ell_{Rk}^2\mathbb{E}\Bigg\{\Bigg|\mathbf{g}_{Rk}^T\text{diag}\Big(\mathbb{E}\left\{\mathbf{W}\left(\alpha^2(p_s\mathbf{h}_{SR}\mathbf{h}_{SR}^H+\sigma_R^2\mathbf{I}_N)\right.\right. \\ &\quad\left.\left.+\alpha\rho\text{diag}(p_s\mathbf{h}_{SR}\mathbf{h}_{SR}^H+\sigma_R^2\mathbf{I}_N)\right)\mathbf{W}^H\right\}\Big)\mathbf{g}_{Rk}^*\Bigg|\Bigg\} \\ &= \alpha\rho\gamma^2\ell_{Rk}^2\mathbb{E}\Bigg\{\Bigg|\mathbf{g}_{Rk}^T\text{diag}\Big(\mathbb{E}\left\{\alpha^2p_s\mathbf{W}\mathbf{h}_{SR}\mathbf{h}_{SR}^H\mathbf{W}^H\right. \\ &\quad\left.+\alpha\rho p_s\mathbf{W}\text{diag}\left(\mathbf{h}_{SR}\mathbf{h}_{SR}^H\right)\mathbf{W}^H\right\}\Big)\mathbf{g}_{Rk}^*\Bigg|\Bigg\} \\ &\quad+(\alpha^2+\alpha\rho)\rho\gamma^2\ell_{Rk}^2\sigma_R^2.\end{aligned} \tag{67}$$

Applying the results in deriving $\widetilde{C}_k$, (67) can be further simplified as

$$\begin{aligned}\mathbb{E}\left\{D_k\right\} &= \alpha\rho\gamma^2\ell_{Rk}^2\mathbb{E}\Bigg\{\Bigg|\mathbf{g}_{Rk}^T\text{diag}\Big(\mathbb{E}\left\{\alpha^2p_s\ell_{SR}^2N\Psi_{SR}\mathbf{w}_t\mathbf{w}_t^H\right. \\ &\quad\left.+\alpha\rho p_s\ell_{SR}^2p_sN\Psi_{SR}\mathbf{w}_t\mathbf{w}_t^H\right\}\Big)\mathbf{g}_{Rk}^*\Bigg|\Bigg\} \\ &\quad+(\alpha^2+\alpha\rho)\rho\gamma^2\ell_{Rk}^2\sigma_R^2 \\ &= \alpha\rho\gamma^2\ell_{Rk}^2\ell_{SR}^2p_s\left(\alpha^2\mathcal{G}_{SR}^2+\alpha\rho N\Psi_{SR}\right) \\ &\quad+(\alpha^2+\alpha\rho)\rho\gamma^2\ell_{Rk}^2\sigma_R^2.\end{aligned} \tag{68}$$

REFERENCES

[1] S. Dang, O. Amin, B. Shihada, and M.-S. Alouini, "What should 6G be?" *Nature Electron.*, vol. 3, no. 1, pp. 20–29, Jan. 2020.

[2] C. Liu, W. Feng, Y. Chen, C.-X. Wang, and N. Ge, "Cell-free satellite-UAV networks for 6G wide-area Internet of Things," *IEEE J. Sel. Areas Commun.*, vol. 39, no. 4, pp. 1116–1131, Apr. 2021.

[3] B. Mao, F. Tang, Y. Kawamoto, and N. Kato, "Optimizing computation offloading in satellite-UAV-served 6G IoT: A deep learning approach," *IEEE Netw.*, vol. 35, no. 4, pp. 102–108, Jul. 2021.

[4] Q. Huang, M. Lin, J. Wang, T. A. Tsiftsis, and J. Wang, "Energy efficient beamforming schemes for satellite-aerial-terrestrial networks," *IEEE Trans. Commun.*, vol. 68, no. 6, pp. 3863–3875, Jun. 2020.

[5] C. Yin, Z. Xiao, X. Cao, X. Xi, P. Yang, and D. Wu, "Offline and online search: UAV multiobjective path planning under dynamic urban environment," *IEEE Internet Things J.*, vol. 5, no. 2, pp. 546–558, Apr. 2018.

[6] L. Zhu, J. Zhang, Z. Xiao, X. Cao, X.-G. Xia, and R. Schober, "Millimeter-wave full-duplex UAV relay: Joint positioning, beamforming, and power control," *IEEE J. Sel. Areas Commun.*, vol. 38, no. 9, pp. 2057–2073, Sep. 2020.

[7] J. Liu, Y. Shi, Z. M. Fadlullah, and N. Kato, "Space-air-ground integrated network: A survey," *IEEE Commun. Surveys Tuts.*, vol. 20, no. 4, pp. 2714–2741, 4th Quart., 2018.

[8] M. Alzenad, A. El-Keyi, F. Lagum, and H. Yanikomeroglu, "3-D placement of an unmanned aerial vehicle base station (UAV-BS) for energy-efficient maximal coverage," *IEEE Wireless Commun. Lett.*, vol. 6, no. 4, pp. 434–437, Aug. 2017.

[9] J. Lu, S. Wan, X. Chen, Z. Chen, P. Fan, and K. B. Letaief, "Beyond empirical models: Pattern formation driven placement of UAV base stations," *IEEE Trans. Wireless Commun.*, vol. 17, no. 6, pp. 3641–3655, Jun. 2018.

[10] P. Zhan, K. Yu, and A. L. Swindlehurst, "Wireless relay communications with unmanned aerial vehicles: Performance and optimization," *IEEE Trans. Aerosp. Electron. Syst.*, vol. 47, no. 3, pp. 2068–2085, Jul. 2011.

[11] Z. Xiao, H. Dong, L. Bai, D. O. Wu, and X.-G. Xia, "Unmanned aerial vehicle base station (UAV-BS) deployment with millimeter-wave beamforming," *IEEE Internet Things J.*, vol. 7, no. 2, pp. 1336–1349, Feb. 2020.

[12] J. Zhao, F. Gao, Q. Wu, S. Jin, Y. Wu, and W. Jia, "Beam tracking for UAV mounted SatCom on-the-move with massive antenna array," *IEEE J. Sel. Areas Commun.*, vol. 36, no. 2, pp. 363–375, Feb. 2018.

[13] D. Xu, Y. Sun, D. W. K. Ng, and R. Schober, "Multiuser MISO UAV communications in uncertain environments with no-fly zones: Robust trajectory and resource allocation design," *IEEE Trans. Commun.*, vol. 68, no. 5, pp. 3153–3172, May 2020.

[14] L. Zhu, J. Zhang, Z. Xiao, X. Cao, D. O. Wu, and X.-G. Xia, "3-D beamforming for flexible coverage in millimeter-wave UAV communications," *IEEE Wireless Commun. Lett.*, vol. 8, no. 3, pp. 837–840, Jun. 2019.

[15] W. Feng et al., "Joint 3D trajectory and power optimization for UAV-aided mmWave MIMO-NOMA networks," *IEEE Trans. Commun.*, vol. 69, no. 4, pp. 2346–2358, Apr. 2021.

[16] Y. Zhang, Z. Mou, F. Gao, J. Jiang, R. Ding, and Z. Han, "UAV-enabled secure communications by multi-agent deep reinforcement learning," *IEEE Trans. Veh. Technol.*, vol. 69, no. 10, pp. 11599–11611, Oct. 2020.

[17] Y.-W. P. Hong, P.-C. Lan, and C.-C. J. Kuo, "Enhancing physical-layer secrecy in multiantenna wireless systems: An overview of signal processing approaches," *IEEE Signal Process. Mag.*, vol. 30, no. 5, pp. 29–40, Sep. 2013.

[18] X. Chen, C. Zhong, C. Yuen, and H.-H. Chen, "Multi-antenna relay aided wireless physical layer security," *IEEE Commun. Mag.*, vol. 53, no. 12, pp. 40–46, Dec. 2015.

[19] J. Ji, K. Zhu, D. Niyato, and R. Wang, "Joint trajectory design and resource allocation for secure transmission in cache-enabled UAV-relaying networks with D2D communications," *IEEE Internet Things J.*, vol. 8, no. 3, pp. 1557–1571, Feb. 2021.

[20] Y. Cai, Z. Wei, R. Li, D. W. K. Ng, and J. Yuan, "Joint trajectory and resource allocation design for energy-efficient secure UAV communication systems," *IEEE Trans. Commun.*, vol. 68, no. 7, pp. 4536–4553, Jul. 2020.

[21] Q. Yuan, Y. Hu, C. Wang, and Y. Li, "Joint 3D beamforming and trajectory design for UAV-enabled mobile relaying system," *IEEE Access*, vol. 7, pp. 26488–26496, 2019.

[22] H. Wu, Y. Wen, J. Zhang, Z. Wei, N. Zhang, and X. Tao, "Energy-efficient and secure air-to-ground communication with jittering UAV," *IEEE Trans. Veh. Technol.*, vol. 69, no. 4, pp. 3954–3967, Apr. 2020.

[23] M. Hua, Y. Wang, Q. Wu, H. Dai, Y. Huang, and L. Yang, "Energy-efficient cooperative secure transmission in multi-UAV-enabled wireless networks," *IEEE Trans. Veh. Technol.*, vol. 68, no. 8, pp. 7761–7775, Jun. 2019.

[24] G. Yang, R. Dai, and Y.-C. Liang, "Energy-efficient UAV backscatter communication with joint trajectory design and resource optimization," *IEEE Trans. Wireless Commun.*, vol. 20, no. 2, pp. 926–941, Feb. 2021.
[25] L. Zhao, M. Li, C. Liu, S. V. Hanly, I. B. Collings, and P. A. Whiting, "Energy efficient hybrid beamforming for multi-user millimeter wave communication with low-resolution A/D at transceivers," *IEEE J. Sel. Areas Commun.*, vol. 38, no. 9, pp. 2142–2155, Sep. 2020.
[26] E. Vlachos and J. Thompson, "Energy-efficiency maximization of hybrid massive MIMO precoding with random-resolution DACs via RF selection," *IEEE Trans. Wireless Commun.*, vol. 20, no. 2, pp. 1093–1104, Feb. 2021.
[27] R. H. Walden, "Analog-to-digital converter survey and analysis," *IEEE J. Sel. Areas Commun.*, vol. 17, no. 4, pp. 539–550, Apr. 1999.
[28] C. Kong, A. Mezghani, C. Zhong, A. L. Swindlehurst, and Z. Zhang, "Multipair massive MIMO relaying systems with one-bit ADCs and DACs," *IEEE Trans. Signal Process.*, vol. 66, no. 11, pp. 2984–2997, Mar. 2018.
[29] F. Sohrabi, Y.-F. Liu, and W. Yu, "One-bit precoding and constellation range design for massive MIMO with QAM signaling," *IEEE J. Sel. Topics Signal Process.*, vol. 12, no. 3, pp. 557–570, Jun. 2018.
[30] Z. Cheng, B. Liao, Z. He, and J. Li, "Transmit signal design for large-scale MIMO system with 1-bit DACs," *IEEE Trans. Wireless Commun.*, vol. 18, no. 9, pp. 4466–4478, Sep. 2019.
[31] Y.-Y. Jeong, S.-H. Ahn, J. Koh, and W.-S. Lee, "Printed dipole antenna array with reconfigurable feeding network for wide elevation angle of U2X communications," *IEEE Access*, vol. 10, pp. 39193–39203, 2022.
[32] Z. Xiao et al., "A survey on millimeter-wave beamforming enabled UAV communications and networking," *IEEE Commun. Surveys Tuts.*, vol. 24, no. 1, pp. 557–610, 1st Quart., 2022.
[33] K.-U. Storek and A. Knopp, "Fair user grouping for multibeam satellites with MU-MIMO precoding," in *Proc. IEEE Global Commun. Conf.*, Dec. 2017, pp. 1–7.
[34] S. Yan and R. Malaney, "Location-based beamforming for enhancing secrecy in Rician wiretap channels," *IEEE Trans. Wireless Commun.*, vol. 15, no. 4, pp. 2780–2791, Apr. 2016.
[35] C. Liu and R. Malaney, "Location-based beamforming and physical layer security in Rician wiretap channels," *IEEE Trans. Wireless Commun.*, vol. 15, no. 11, pp. 7847–7857, Nov. 2016.
[36] J. Mo, P. Schniter, and R. W. Heath Jr., "Channel estimation in broadband millimeter wave MIMO systems with few-bit ADCs," *IEEE Trans. Signal Process.*, vol. 66, no. 5, pp. 1141–1154, Mar. 2018.
[37] C.-J. Wang, C.-K. Wen, S. Jin, and S.-H. Tsai, "Gridless channel estimation for mixed one-bit antenna array systems," *IEEE Trans. Wireless Commun.*, vol. 17, no. 12, pp. 8485–8501, Dec. 2018.
[38] J. Hu, J. Shi, S. Ma, and Z. Li, "Secrecy analysis for orthogonal time frequency space scheme based uplink LEO satellite communication," *IEEE Wireless Commun. Lett.*, vol. 10, no. 8, pp. 4972–4987, Aug. 2021.
[39] W. Cao et al., "Secrecy outage analysis of relay-user pairing for secure hybrid satellite-terrestrial networks," *IEEE Trans. Veh. Technol.*, vol. 71, no. 8, pp. 8906–8918, Aug. 2022.
[40] A. Abdi, W. C. Lau, M.-S. Alouini, and M. Kaveh, "A new simple model for land mobile satellite channels: First- and second-order statistics," *IEEE Trans. Wireless Commun.*, vol. 2, no. 3, pp. 519–528, May 2003.
[41] K. Guo, M. Lin, B. Zhang, W.-P. Zhu, J.-B. Wang, and T. A. Tsiftsis, "On the performance of LMS communication with hardware impairments and interference," *IEEE Trans. Commun.*, vol. 67, no. 2, pp. 1490–1505, Feb. 2019.
[42] R. B. Ertel, P. Cardieri, K. W. Sowerby, T. S. Rappaport, and J. H. Reed, "Overview of spatial channel models for antenna array communication systems," *IEEE Pers. Commun.*, vol. 5, no. 1, pp. 10–22, Feb. 1998.
[43] A. A. Khuwaja, Y. Chen, N. Zhao, M.-S. Alouini, and P. Dobbins, "A survey of channel modeling for UAV communications," *IEEE Commun. Surveys Tuts.*, vol. 20, no. 4, pp. 2804–2821, 4th Quart., 2018.
[44] C. Liu, J. Lee, and T. Q. S. Quek, "Safeguarding UAV communications against full-duplex active eavesdropper," *IEEE Trans. Wireless Commun.*, vol. 18, no. 6, pp. 931–2919, Jun. 2019.
[45] X. Yuan, Z. Feng, W. Ni, R. P. Liu, J. A. Zhang, and W. Xu, "Secrecy performance of terrestrial radio links under collaborative aerial eavesdropping," *IEEE Trans. Inf. Forensics Security*, vol. 15, pp. 604–619, 2020.
[46] A. K. Fletcher, S. Rangan, V. K. Goyal, and K. Ramchandran, "Robust predictive quantization: Analysis and design via convex optimization," *IEEE J. Sel. Topics Signal Process.*, vol. 1, no. 4, pp. 618–632, Dec. 2007.
[47] J. Max, "Quantizing for minimum distortion," *IRE Trans. Inf. Theory*, vol. 6, no. 1, pp. 7–12, Mar. 1960.
[48] P. Dong, H. Zhang, Q. Wu, and G. Y. Li, "Spatially correlated massive MIMO relay systems with low-resolution ADCs," *IEEE Trans. Veh. Technol.*, vol. 69, no. 6, pp. 6541–6553, Jun. 2020.
[49] Y. Li, C. Tao, G. Seco-Granados, A. Mezghani, A. L. Swindlehurst, and L. Liu, "Channel estimation and performance analysis of one-bit massive MIMO systems," *IEEE Trans. Signal Process.*, vol. 65, no. 15, pp. 4075–4089, Apr. 2017.
[50] I. Atzeni and A. Tolli, "Channel estimation and data detection analysis of massive MIMO with 1-bit ADCs," *IEEE Trans. Wireless Commun.*, vol. 21, no. 6, pp. 3850–3867, Jun. 2022.
[51] M. Bloch, J. Barros, M. R. D. Rodrigues, and S. W. McLaughlin, "Wireless information-theoretic security," *IEEE Trans. Inf. Theory*, vol. 54, no. 6, pp. 2515–2534, Jun. 2008.
[52] R. Zhao, Y. Huang, W. Wang, and V. K. Lau, "Ergodic achievable secrecy rate of multiple-antenna relay systems with cooperative jamming," *IEEE Trans. Wireless Commun.*, vol. 15, no. 4, pp. 2537–2551, Apr. 2016.
[53] Q. Zhang, S. Jin, K.-K. Wong, H. Zhu, and M. Matthaiou, "Power scaling of uplink massive MIMO systems with arbitrary-rank channel means," *IEEE J. Sel. Topics Signal Process.*, vol. 8, no. 5, pp. 966–981, Oct. 2014.
[54] I. S. Gradshteyn and I. M. Ryzhik, *Table of Integrals, Series, and Products*, 7th ed., San Diego, CA, USA: Academic, 2007.
[55] P. K. Upadhyay and P. K. Sharma, "Max-max user-relay selection scheme in multiuser and multirelay hybrid satellite-terrestrial relay systems," *IEEE Commun. Lett.*, vol. 20, no. 2, pp. 268–271, Feb. 2016.
[56] R. Hunger, "Floating point operations matrix-vector calculus," Technische Univ. Munchen, Associate Inst. Signal Process., Munich, Germany, Tech. Rep., TUM-LNS-TR-05-05, Oct. 2005.
[57] G. Chen, J. P. Coon, and M. Di Renzo, "Secrecy outage analysis for downlink transmissions in the presence of randomly located eavesdroppers," *IEEE Trans. Inf. Forensics Security*, vol. 12, no. 5, pp. 1195–1206, May 2017.
[58] X. Fang et al., "NOMA-based hybrid satellite-UAV-terrestrial networks for 6G maritime coverage," *IEEE Trans. Wireless Commun.*, early access, Jul. 25, 2022, doi: 10.1109/TWC.2022.3191719.
[59] L. Chu, F. Wen, L. Li, and R. Qiu, "Efficient nonlinear precoding for massive MIMO downlink systems with 1-bit DACs," *IEEE Trans. Wireless Commun.*, vol. 18, no. 9, pp. 4213–4224, Sep. 2019.
[60] A. Cika, M.-A. Badiu, and J. P. Coon, "Statistical properties of transmissions subject to Rayleigh fading and Ornstein-Uhlenbeck mobility," *IEEE Trans. Mobile Comput.*, vol. 21, no. 1, pp. 332–341, Jan. 2022.
[61] N. Ravindran, N. Jindal, and H. C. Huang, "Beamforming with finite rate feedback for LOS MIMO downlink channels," in *Proc. IEEE Global Commun. Conf. (GLOBECOM)*, Nov. 2007, pp. 4200–4204.

Dongxuan He received the B.S. degree in automation and the Ph.D. degree in information and communication systems from the Beijing Institute of Technology (BIT) in 2013 and 2019, respectively. From 2017 to 2018, he was a Visiting Student at the Singapore University of Technology and Design (SUTD). From 2019 to 2022, he was a Post-Doctoral Researcher at the Department of Electronic Engineering, Tsinghua University. He is currently an Assistant Professor with the School of Information and Electronics, BIT. His current research interests include terahertz communication, AI empowered wireless communications, and physical layer security. He was also an Exemplary Reviewer of IEEE WIRELESS COMMUNICATIONS LETTERS.

Ziyuan Sha received the B.S. and Ph.D. degrees from the Department of Electronic Engineering, Tsinghua University, Beijing, China, in 2017 and 2022, respectively. He is currently with Zeku Technology Corporation Ltd., Beijing. His main research interests include signal processing and resource management techniques in millimeter wave and terahertz communications.

Han Liu received the M.S. degree in digital communication system from the University of Sussex, Brighton, U.K., in 2013, and the Ph.D. degree in information and electronics from the Beijing Institute of Technology, Beijing, China, in 2018. She is currently a Post-Doctoral Research Fellow with the School of Information and Electronics, Beijing Institute of Technology. Her research interests include signal processing, object detection, and physical layer security.

Tianqi Mao (Member, IEEE) received the B.S., M.S. (Hons.), and Ph.D. (Hons.) degrees from Tsinghua University in 2015, 2018, and 2022, respectively. Since 2022, he has been a Research Fellow with the School of Electronic and Information Engineering, Beihang University, Beijing, China. He has authored over 20 IEEE/OSA journals and conference papers in IEEE COMMUNICATIONS SURVEYS AND TUTORIALS, IEEE JOURNAL ON SELECTED AREAS IN COMMUNICATIONS, IEEE WIRELESS COMMUNICATIONS, *IEEE Communications Magazine*, IEEE TRANSACTIONS ON COMMUNICATIONS, and IEEE TRANSACTIONS ON VEHICULAR TECHNOLOGY, including two highly cited papers of ESI (as the first author). His current research interests include modulation and signal processing for wireless communications, terahertz communications, near-space wireless communications, and visible light communications. He was a recipient of the 8th Young Elite Scientists Sponsorship Program by China Association for Science and Technology, the Science and Technology Award (Second Prize) of China Institute of Communications, the Excellent Master Dissertation of Chinese Institute of Electronics, the Special Scholarship of Tsinghua University, the Outstanding Ph.D. Graduate of Beijing, and the Outstanding Master Graduate of Tsinghua University. He is also an Associate Editor of IEEE COMMUNICATIONS LETTERS and a Guest Editor of IEEE OPEN JOURNAL OF THE COMMUNICATIONS SOCIETY. He was also the Exemplary Reviewer of IEEE TRANSACTIONS ON COMMUNICATIONS and IEEE COMMUNICATIONS LETTERS.

Zhaocheng Wang (Fellow, IEEE) received the B.S., M.S., and Ph.D. degrees from Tsinghua University in 1991, 1993, and 1996, respectively.

From 1996 to 1997, he was a Post-Doctoral Fellow with Nanyang Technological University, Singapore. From 1997 to 1999, he was a Research Engineer/Senior Engineer with OKI Techno Centre (Singapore) Pte. Ltd., Singapore. From 1999 to 2009, he was a Senior Engineer/ Principal Engineer with Sony Deutschland GmbH, Germany. Since 2009, he has been a Professor with the Department of Electronic Engineering, Tsinghua University, where he is currently the Director of the Broadband Communication Key Laboratory, Beijing National Research Center for Information Science and Technology (BNRist). He has authored or coauthored two books, which have been selected by IEEE Series on Digital and Mobile Communication and published by Wiley-IEEE Press. He has authored/coauthored more than 190 peer-reviewed journal articles. He holds 60 U.S./European granted patents (23 of them as the first inventor). His research interests include wireless communications, millimeter wave communications, optical wireless communications, and AI empowered wireless communications. He is a fellow of the Institution of Engineering and Technology. He was a recipient of ICC2013 Best Paper Award, OECC2015 Best Student Paper Award, 2016 IEEE Scott Helt Memorial Award, 2016 IET Premium Award, 2016 National Award for Science and Technology Progress (First Prize), ICC2017 Best Paper Award, 2018 IEEE ComSoc Asia-Pacific Outstanding Paper Award, and 2020 IEEE ComSoc Leonard G. Abraham Prize. He is also an Associate Editor of IEEE TRANSACTIONS ON COMMUNICATIONS IEEE/OSA JOURNAL OF LIGHTWAVE TECHNOLOGY, IEEE SYSTEMS JOURNAL, and IEEE OPEN JOURNAL OF VEHICULAR TECHNOLOGY. He was an Associate Editor of IEEE TRANSACTIONS ON WIRELESS COMMUNICATIONS from 2011 to 2015 and an Associate Editor of IEEE COMMUNICATIONS LETTERS from 2013 to 2016.